Sustainable Energy & Fuels

ROYAL SOCIETY OF CHEMISTRY

PAPER

View Article Online
View Journal | View Issue

Cite this: *Sustainable Energy Fuels*, 2020, **4**, 4137

Charge transfer characteristics of fullerene-free polymer solar cells *via* multi-state electronic coupling treatment†

Tuuva Kastinen * and Terttu I. Hukka *

Recently, non-fullerene (NF) polymer solar cells (PSCs), where new electron acceptor (eA) materials are blended with a donor–acceptor (D–A) copolymer as an electron donor (eD), have shown promising power conversion efficiencies up to 18%. Some of the best-performing NF PSCs use the eD copolymers **PBDT-TzBI**, **PDTB-EF-T**, and **PBDB-T-2F**, and either a D–A copolymer **P(NDI2OD-T2)** or small molecule acceptors (SMAs) **ITIC-4F** and **ITIC-2Cl** as the NF eA compounds. Here we investigate these systems with density functional theory methods and extend our previous study of the multi-state fragment charge difference (FCD) electronic coupling scheme by applying it to the calculations of charge transfer (CT) rates for exciton dissociation and charge recombination (CR) processes at local eD–eA interfaces. Despite similar backbone structures and optical properties, the studied eD copolymers have different conformational, ionization, excitation, and CT characteristics. The electronic couplings and CT rates depend strongly on the relative positioning of the eD and eA compounds in the eD–eA complexes. While the main CT path is from eD to the eA compound, CT from eA to the eD compound is also predicted in the polymer–polymer **PBDT-TzBI**–**P(NDI2OD-T2)** system. The multi-state FCD electronic couplings are independent of the number of the excited states included in the calculations when using a dispersion-corrected optimally tuned long-range corrected functional. The calculated CR rates are slower in the polymer–SMA systems than in the polymer–polymer system, which could partly account for their higher experimentally observed efficiencies in devices.

Received 25th February 2020
Accepted 7th June 2020

DOI: 10.1039/d0se00306a

rsc.li/sustainable-energy

Introduction

Polymer solar cells (PSCs) have a great potential as a low-cost, lightweight, flexible, and scalable technology for light conversion.[1,2] So far, the most studied systems have included fullerene derivatives as the electron acceptor (eA) materials with conjugated donor–acceptor (D–A) copolymers as the electron donor (eD) materials. Although these fullerene-based PSCs have achieved promising power conversion efficiencies (PCEs) of *ca.* 12%,[3,4] they possess several hindrances, such as limited possibilities to tune the chemical structures and energy levels of fullerene derivatives, high synthesis cost, poor light absorption in the visible and infrared spectral regions, and morphological instabilities.[5,6] To overcome these limitations, the researchers have developed alternative eA materials with tunable structural and optoelectronic features, which can be matched with a wider range of eD copolymers. As a consequence, a rapid and encouraging progress has been made in designing fullerene-free, *i.e.* non-fullerene (NF) PSCs during the past few years.[5,7]

In all-polymer solar cells (APSCs), D–A copolymers composed of electron-rich donor and electron-deficient acceptor units in the constitutional repeating unit (CRU) are employed as both the eD and eA materials. This type of a design strategy[8,9] has enabled fine-tuning of the structural and optoelectronic properties, *e.g.* ionization energies (IE), electron affinities (EA), and optical gaps, of the D–A copolymers by selecting the backbone donor and acceptor units with the desirable characteristics.[10] Controlling these features for the eA compounds can yield APSC devices with improved light absorption, higher open-circuit voltage, and enhanced long-term stability compared to the conventional, fullerene-based PSCs.[5] Especially, naphthalene diimide (NDI) based copolymers have been popular eA materials in APSCs due to their large EAs, high electron mobilities,

Chemistry and Advanced Materials, Faculty of Engineering and Natural Sciences, Tampere University, P.O. Box 541, FI-33014 Tampere, Finland. E-mail: tuuva.kastinen@tuni.fi; terttu.hukka@tuni.fi; Tel: +358 40 198 1133

† Electronic supplementary information (ESI) available: More details on the construction of the eD–eA complexes. Additional information regarding the methods. The following details on the results: the OT ω for the individual eD and eA compounds and the eD–eA complexes. Relaxed PES scans of the selected dihedrals in the monomer models of the eD and eA copolymers and **ITIC**. The BLA_{total} values of the eD and eA compounds and bond length differences between the geometries of the charged (radical and S_1) and neutral (GS) eD and eA compounds in vacuum and $CHCl_3$. Additional optoelectronic properties (HOMO, LUMO, and HOMO–LUMO gap energies, IEs, EAs, vertical excitation energies, oscillator strengths, and UV-vis absorption spectra) of the eD and eA compounds. The optimized geometries and relative energies of the eD–eA complexes. The multi-state FCD electronic couplings, additional CT parameters, and rates of the eD–eA complexes. See DOI: 10.1039/d0se00306a

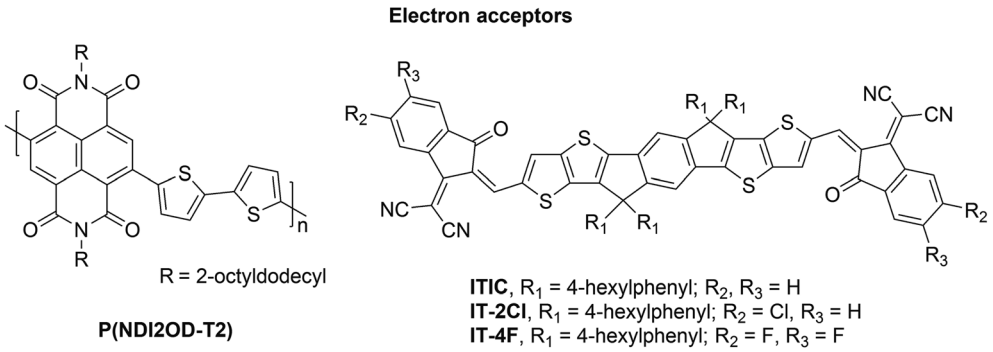

Fig. 1 Molecular structures of the studied eA compounds.

and good thermal and oxidative stabilities.[11,12] The highest PCEs have been *ca.* 12%[13,14] for APSCs using poly[(*N*,*N*′-bis(2-octyldodecyl)naphthalene-1,4,5,8-bis(dicarboximide)-2,6-diyl)-*alt*-5,5′-(2,2′-bithiophene)] (**P(NDI2OD-T2)**, also referred to as N2200) as the eA material[15] (Fig. 1). These efficiencies have been surpassed recently with a new eA copolymer (PJ1), which is based on a small molecule acceptor (SMA) building block leading to the PCE of 14.4%.[16]

Another emerging type of the efficient NF PSCs makes use of π-conjugated SMAs as the eA materials, whose acceptor–donor–acceptor (A–D–A) structure leads to strong intramolecular electron push–pull effects similar to the ones in D–A copolymers. For example, in a successful **ITIC**,[17] an electron-donating, bulky seven-ring indacenodithieno[3,2-*b*]thiophene (IT) core is end-capped with electron-withdrawing 2-(3-oxo-2,3-dihydroinden-1-ylidene)malononitrile (INCN) groups. This type of a rigid A–D–A structured backbone results in the extended conjugation and reduces reorganization energy, which is beneficial for charge transport.[17,18] However, on the downside, planar backbones with the extended conjugation may lead to the undesired aggregation behavior for **ITIC** (and other SMAs) and consequently decreased efficiencies of PSCs. Thus, four 4-hexylphenyl have been substituted to the IT core to restrict the planarity and consequently aggregation of **ITIC** in blend films. The advantages of **ITIC** derivatives are strong light absorption and good electron mobility. Furthermore, their properties can be easily tuned *via* molecular modifications, while simultaneously maintaining their key aspects of efficient eAs.[19,20] For example, NF-SMA PSCs based on **ITIC** derivatives with halogenated (*e.g.* fluorinated or chlorinated) end groups have some of the highest

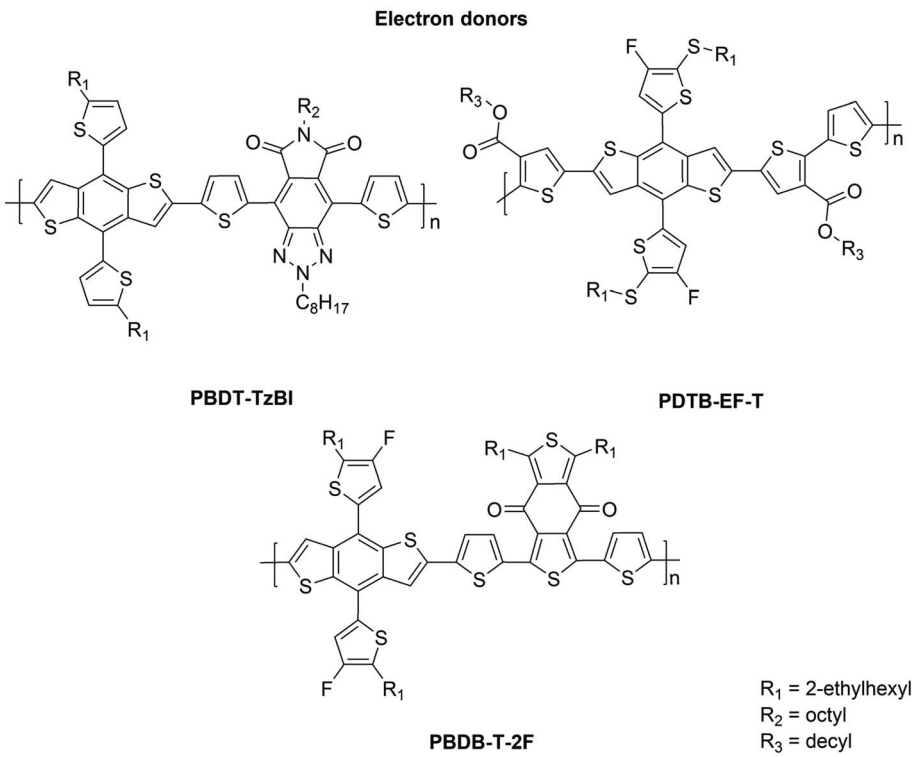

Fig. 2 CRUs of the studied eD copolymers.

PCEs (*ca.* 15%) for PSCs.[21–23] The record PCEs (*ca.* 18%[24]) for the NF PSCs have been achieved recently with a SMA[25] (Y6) consisting of dithienothiophen[3.2-*b*]-pyrrolobenzothiadiazole core and 2-(5,6-difluoro-3-oxo-2,3-dihydro-1*H*-inden-1-ylidene) malononitrile side groups.

The NF eA materials discussed above have either small (*i.e.* below 1.50 eV; *ca.* 1.48 eV for **P(NDI2OD-T2)**) or medium (*i.e.* 1.50–1.90 eV; *ca.* 1.60 eV for **ITIC**) bandgaps.[26] Thus, to achieve a wide absorption of the solar spectrum and efficient NF PSCs, they are typically combined with medium- or wide-bandgap (>1.9 eV) copolymers as the eD compounds. These kinds of copolymers (Fig. 2) include poly[4,8-bis(5-(2-ethylhexyl)thiophen-2-yl)benzo[1,2-*b*:4,5-*b*′]dithiophene-*co*-4,8-di(thien-2-yl)-6-octyl-2-octyl-5*H*-pyrrolo[3,4-*f*]benzotriazole-5,7(6*H*)-dione] (referred to as **PBDT-TzBI** in this work; known also as PTzBI[27] or PTZBIBDT[28]), **PDTB-EF-T**,[29] and poly[(2,6-(4,8-bis(5-(2-ethylhexyl)-4-fluorothiophen-2-yl)benzo[1,2-*b*:4,5-*b*′]dithiophene))-*alt*-(5,5-(1′,3′-bis(thiophen-2-yl)-5′,7′-bis(2-ethylhexyl)benzo [1′,2′-*c*:4′,5′-*c*′]dithiophene-4,8-dione))],[30,31] see the ref. 32 for the alternative naming (referred to as **PBDB-T-2F** [33] in this work; known also as **PBDB-TF**[21] or PM6 [31]). Among these eDs, **PBDT-TzBI**[28] and **PBDB-T-2F**[31] have been originally developed for fullerene-based PSCs.

All of the aforementioned copolymers have the same weak, electron-rich donor unit, benzo[1,2-*b*:4,5-*b*′]dithiophene (BDT), but different electron-deficient acceptor units, TzBI in **PBDT-TzBI**[28] and 1,3-bis(thiophen-2-yl)-5,7-bis(2-ethylhexyl)benzo[1,2-*c*:4,5-*c*′]dithiophene-4,8-dione (BDD)[34,35] in **PBDB-T-2F**. In addition, there are thiophene spacers between the donor and acceptor units, which have a role in controlling planarity, and accordingly, aggregation.[36] The introduction of thiophenes in the copolymer backbone also weakens the intramolecular charge transfer (CT) character between the donor and acceptor units, which leads to the medium or wide band gaps in these copolymers.[37] In **PDTB-EF-T**, the thiophenes with the electron-withdrawing ester groups have been used instead of a strong electron-deficient unit.[29] Additionally, the desired IEs, EAs and structural characteristics of these copolymers have been achieved by attaching different functional groups, such as aromatic rings (*e.g.* thiophene) and electronegative atoms, *e.g.* fluorine,[29,31,33,38] to their backbones.

Theoretical quantum chemical calculations provide means for determining intrinsic structure–property relationships of π-conjugated PSC materials. Moreover, they can provide insight into the CT processes taking place at local interfaces of the eD and eA compounds. So far, there have been a number of studies on structural and optoelectronic properties of individual NF PSC compounds with density functional theory (DFT) methods.[25,39–42] For example, Wang *et al.* have investigated both the electronic and optical properties of two NF SMAs (IDIC and IDTBR) and five D–A copolymers and their interfacial characteristics.[41] The effect of fluorination on the characteristics of the eD copolymers and **ITIC** has been examined by Benatto *et al.*[43] Local interfaces in the NF devices have been exploited, as well.[23,41,44–49] Han *et al.* have studied the impact of different eD molecular architectures on the interfacial arrangements and electronic properties of the NF organic solar cells based on small-molecule eDs and the SMA **ITIC-4F** with the multiscale simulations combining molecular dynamics (MD) and DFT calculations.[45] Moreover, they have compared the interfacial complexes consisting of **PBDB-T-2F** as the eD copolymer and either $PC_{71}BM$ or **ITIC** as the eA compound with both MD and DFT.[44] The NF PSC systems of **PBDB-T-2F** and different **ITIC** derivatives have been the subject of other MD simulations, as well.[46–49] Han *et al.* have also compared the packing of the **ITIC** and $PC_{71}BM$ acceptor thin films with MD simulations.[50] While these studies have included electronic structure calculations of some of the aforementioned efficient NF PSC compounds, they have mostly concentrated on the MD simulations of the blend morphologies, and thus a deeper understanding of the electronic structure–function relations and CT characteristics of these compounds is still required.

For the efficient charge generation in PSCs, the rates of exciton dissociation (ED) should be maximized, whereas the rates of charge recombination (CR) should be minimized.[51] In the previous theoretical studies of the NF PSCs systems, the ED and CR rates have also been evaluated to gain deeper understanding of these CT pathways.[47–49] The electronic coupling (H_{if}) between the initial (i) and final (f) charge-localized, *i.e.* diabatic states is one of the key parameters defining the CT rates.[52] Number of different theoretical approaches have been developed for calculating the couplings.[53–55] In the studies of polymer–fullerene-based PSC systems, the two-state fragment charge difference (FCD)[56] and generalized Mulliken–Hush (GMH)[57,58] schemes have been popular choices.[59–62] However, if a component of the local excitation is mixing with the CT state of interest, multiple adiabatic states should be included to obtain a more accurate description of the diabatic states.[63,64] In our previous studies,[65,66] we have observed the tendency of the long-range-corrected (LRC) functionals to predict mixed CT states for the polymer–fullerene systems. Our latest study[66] showed that use of the multi-state FCD and GMH schemes[64] with both the non-tuned and optimally-tuned (OT) LRC functionals reduces this mixing. In the previous studies of the NF PSC systems, the GMH scheme has been applied in conjunction with the (non-tuned) LRC functional CAM-B3LYP for **PBDB-T**–**ITIC**[47,48] and with the OT-ωB97X-D functional for **PBDB-T**–ITOM.[49] However, the FCD scheme, which we observed[66] to be less sensitive to the number of states and the choice of the calculation method compared to GMH, does not seem to have been applied for the NF PSC systems yet. Furthermore, it is beneficial to investigate, whether the inclusion of multiple states effects the electronic couplings of the NF PSC systems. Information regarding the effect of the dispersion corrections included in the DFT functional on the multi-state coupling calculations is still missing, as well.

In this work, we will investigate *via* DFT and time-dependent DFT (TDDFT) methods a selected set of eD (Fig. 2) and eA (Fig. 1) compounds, which have been recently employed in some of the most efficient NF PSCs.[6,27,29,33,67] The selected eD compounds include D–A copolymers **PBDT-TzBI**, **PDTB-EF-T**, and **PBDB-T-2F**, whereas for the eA compounds, the D–A copolymer **P(NDI2OD-T2)**, the SMA **ITIC**, and its fluorinated and chlorinated counterparts, **ITIC-4F** and **ITIC-2Cl**, respectively,

have been chosen. We use theory to shed light on those characteristics that make the selected compounds successful and on the CT processes that take place at their local eD–eA interfaces. The first part of the work will explore the structural, ionization, excitation, and optoelectronic properties of the individual eD and eA compounds. In the second part, we will examine the local interfacial configurations, CT characteristics, and CT rates for the ED (eD*–eA → eD^+–eA^-) and CR (eD^+–eA^- → eD–eA) processes of the corresponding eD–eA complexes. For obtaining the CT rates, we utilize the multi-state FCD scheme to calculate the electronic couplings. This work extends our previous study[66] of the effects of the two- *versus* multi-state treatments on electronic couplings in fullerene-based PSC systems by exploring the influence of multiple states and dispersion corrections on coupling values of the studied NF PSCs. Based on our[65] and other's findings[68,69] on organic solar cell systems, dispersion corrections are important for describing weak dispersion interactions at their local eD–eA interfaces. Furthermore, tuned LRC functionals have performed well in calculations of both the individual PSC compounds[70,71] and local interfaces.[65,66] Thus, the OT version of the dispersion corrected LRC functional ωB97X-D[72] was selected to investigate the effects of both the tuning of a LRC functional and dispersion corrections on the electronic coupling values. In some of the TDDFT calculations, we employ also the global hybrid PBE0 [73–75] functional for comparison.

Computational details

Models

The eD and eA compounds studied here (see Fig. 1 and 2) comprise both of the D–A copolymers (**PBDT-TzBI**, **PDTB-EF-T**, **PBDB-T-2F**, and **P(NDI2OD-T2)**) and the A–D–A-type SMAs (**ITIC**, **ITIC-2Cl**, and **ITIC-4F**). In most calculations, the full-length side chains of the compounds were replaced by methyl groups to reduce the computational cost, except for some of the relaxed potential energy surface (PES) scans of the side groups to check the dihedral angles within the side groups and between the side groups and the backbone donor or acceptor units. We note, however, that long alkyl side chains affect the solid-state packing and resulting optoelectronic characteristics,[76] and they should be included, *e.g.* when the atomistic simulations of blends are carried out.

The eD and eA copolymer models are defined by their CRUs (*i.e.* the repeating units, *n*). A CRU consists of donor and acceptor units and additional thiophene spacers. The monomer and oligomer models of the copolymers consist of 1–4 CRUs and will be referred to as **BDT-TzBI**, **DTB-EF-T**, **BDB-T-2F**, and **NDI2OD-T2** (without P in front). The relative orientations of their backbone units were selected based on the relaxed PES scans (see Methods below and Fig. S1–S3† for the studied dihedrals). Within the CRU of a D–A copolymer, neighboring donor and acceptor units can be either *anti* to each other, *i.e.* the neighboring heteroatoms of the units are on the opposite sides, or *syn* to each other, *i.e.* the neighboring heteroatoms are on the same side. Similarly, the neighboring CRUs can be either *anti* or *syn* with respect to each other. In the text, the conformations are referred to as: *anti*/*anti* or *anti*–*anti*/*anti*, where the first word (or words) refers to the conformation(s) within one CRU and the second word to the conformation between two CRUs. Here, we have considered only the energetically most stable conformations for each copolymer.

Monomer models (*i.e.* hydrogen-terminated CRUs, $n = 1$) of the D–A copolymers were used in the PES calculations to determine the optimal dihedral angles within the backbone. Furthermore, the monomers were employed in the eD–eA complexes (see below). In the studies of the structural, ionization, and excitation characteristics of the individual eD and eA compounds, trimers ($n = 3$) were used as the oligomeric models of the D–A copolymers. As an exception, **P(NDI2OD-T2)** was modeled using a tetramer ($n = 4$) to keep the relative conjugation lengths (*i.e.* the number of the double bonds, *N*, within the shortest path between the terminal carbon atoms of the backbone) in the copolymer models consistent with each other.

The eD–eA complexes were constructed using the optimized GS geometries of the monomer models of the eD and eA copolymers and the **ITIC**-based eA compounds. In addition, dimer models of both the eD copolymer **PBDT-TzBI** and eA copolymer **P(NDI2OD-T2)** were used in one complex configuration to study the effect of a longer oligomer on the local structure and CT characteristics at the eD–eA interface. In all complexes, the eD models were oriented in the *xy* plane along the *x* axis. Three configurations of each complex were studied: the eA model was positioned above the donor, thiophene, and acceptor unit of the eD model along the *x* axis by superposing the centroids of the specific heterocyclic aromatic rings with the initial intermolecular distance of 4 Å (see the ESI† for further information of construction of different configurations). After this, the complexes were fully optimized without any constraints (see Methods).

Methods

All the calculations were carried out with the Gaussian 16 Rev.B01 suite of programs,[77] except for the electronic coupling calculations of the complexes, which were carried out with the Q-Chem 4.2 software.[78] The LRC ωB97X-D functional[72] was selected, as it includes the dispersion corrections and is recommended for studying systems with extended π-conjugated structures.[68]

To determine the relative orientations of the backbone units in the eD and eA compounds for the further calculations, the torsional potentials between the adjacent units within the monomer models of the eD and eA copolymers and the eA compound **ITIC** in their neutral GS geometries were determined with the relaxed PES scans at the ωB97X-D/6-31G** level of theory in vacuum (with the default range-separation parameter, ω, of 0.2 $bohr^{-1}$). The PES scans were carried out also for the dihedral angles between the BDT donor unit and the full-length alkyl thiophene side groups of the eD models (**BDT-TzBI**, **DTB-EF-T**, and **BDB-T-2F**) in addition to those between the BDD acceptor unit and alkyl side chains of **BDB-T-2F** to check their relative orientations (Fig. S3†). The constrained geometry optimizations were carried out at 5° intervals, *i.e.* the studied

dihedral angle was kept fixed while fully optimizing the geometry of the rest of the compound.

For all the other DFT and TDDFT calculations, the optimally tuned dispersion corrected functional, OT-ωB97X-D, was used with the 6-31G** basis set, unless stated otherwise (see the next paragraph). For this purpose, the ω value in ωB97X-D was optimally tuned in vacuum with the gap tuning procedures for the individual eD and eA compounds[79,80] (eqn (S1) in ESI†) and the eD–eA complexes[65,66,80,81] (eqn (S2) in ESI†). The OT ω values were determined with an accuracy of 0.01 $bohr^{-1}$ using the 6-31G** basis set. The GS geometries of the neutral eD and eA compounds and their radicals, *i.e.* cations and anions, were fully optimized with DFT. In the characterization of the individual compounds, calculations were carried out in vacuum, solvent, and blend environments, unless stated otherwise. Solvation effects were included by means of the conductor-like polarizable continuum model (CPCM)[82,83] using the static (ε_s) and dynamic (*i.e.* optical, ε_{op}) dielectric constants of 4.7113 and 2.090627, respectively, for $CHCl_3$. For the blend environment, the ε_s and ε_{op} of 4.00 and 2.25 were used, respectively, which are approximate values employed in previous studies for different organic semiconductors.[84,85] For studying ionization of the eD and eA compounds, their vertical and adiabatic ionization energies (IEs, VIE and AIE) and electron affinities (EAs, VEA and AEA) were calculated with eqn (S3)–(S6) (ESI†). The intramolecular reorganization energies for the hole (λ_h) and electron (λ_e) transfer of the eD and eA compounds were calculated with eqn (S7) and (S8).†

For examining the intramolecular CT character of the NF PSC compounds and determining their UV-vis absorption spectra, the vertical excitation energies for the 10 lowest excited singlet states of the isolated eD and eA compounds were carried out with TDDFT. For the **ITIC** derivatives, the vertical excitations for the 20 lowest excited singlet states were required to yield the best description of the UV-vis spectra. Additionally, the TDDFT calculations of the individual eD and eA compounds were carried out in $CHCl_3$ at the PBE0/6-31G** level of theory using the OT-ωB97X-D-optimized geometries for comparing with the OT-ωB97X-D calculated spectra. The graphical illustrations of the UV-vis absorption spectra were created *via* convolution of the calculated singlet vertical transition energies and oscillator strengths using a Gaussian-shape broadening with a full width at half-maximum (FWHM) of 0.30 eV.

The nature of the excited states for both the individual NF PSC compounds and their complexes was described using natural transition orbitals (NTOs)[86] as a representation for the transition density matrix. The NTOs for the complexes were obtained from the TDDFT calculations carried out with Q-Chem, whereas the NTOs of the individual compounds were generated from the TDDFT calculations using Gaussian. Only the dominant pairs of the NTOs, *i.e.* those with the largest eigenvalues (λ_{NTO}) indicating the fraction of a particular hole–electron excitation to the overall transition,[86,87] were considered. In the case of the individual compounds, the contributions of the backbone units to the NTOs were determined using the C-Squared Population Analysis (C-SPA)[88] as implemented in Multiwfn 3.6.[89–91] For the eD–eA complexes, the nature of the states was determined from the pictorial presentations of the NTOs and calculating the contributions of the eD and eA compounds to the NTOs by using the C-SPA within a self-made code. Pictorial presentations of the geometries and NTOs were generated using ChemCraft 1.8.[92]

The CT rates for the ED and CR processes taking place at the local interfacial complexes were calculated with the semi-classical Marcus theory:[93–95]

$$k_{ED/CR} = \frac{|H_{if}|^2}{\hbar}\sqrt{\frac{\pi}{\lambda k_B T}}\exp\left[-\frac{(\Delta G^\circ + \lambda)^2}{4\lambda k_B T}\right], \quad (1)$$

where H_{if} is the electronic coupling between the initial and final states of the CT process considered;[96] k_B and $\hbar$ are the Boltzmann and reduced Planck constants, respectively; T is temperature (293.15 K here); λ the (intermolecular) reorganization energy (with the inner, λ_i, and outer, λ_i contributions, see eqn (S9) in ESI†); and ΔG° the Gibbs free energy. For calculating the inner reorganization energy, λ_i (eqn (S10)–(S15) in ESI†), and ΔG° (eqn (S16)–(S19) in ESI†), the geometries of the lowest excited singlet states (S_1) of the isolated eD monomers were optimized with TDDFT and those of the radicals (cations of these eD monomers and the anions of the eA compounds) were optimized with DFT. For defining the electronic couplings, vertical excitation energies, and adiabatic charge differences for the 10 lowest excited singlet states of the eD–eA complexes were calculated using TDDFT in the FCD scheme,[56] which is incorporated in the Q-Chem 4.2 software.[78] For the complexes of the polymer–polymer system of **PBDT-TzBI** and **P(NDI2OD-T2)**, the 25 lowest excited singlet states were considered. The two-state FCD coupling values (see eqn (S20) and (S21)†) obtained from the Q-Chem calculations were taken directly, whereas the electronic couplings with multiple states (>2) were determined with the multi-state version of FCD[64] in accordance with our previous work[66] (for further details, see eqn (S22)–(S25) in ESI†).

Results and discussion

Ground-state structural properties of the eD and eA compounds

To better understand the characteristics of the studied NF PSC compounds, we begin by exploring the geometrical structures of the individual eD oligomers and eA compounds. The shapes and sizes of the π-conjugated donor and acceptor units and the inclusions of the additional spacer units between them are among the factors defining the shapes of the backbones of both the D–A copolymers[97] and SMAs.[98] In addition, conformational preferences and resulting torsions induced by weak non-bonding interactions[99] between heteroatoms and between heteroatoms and hydrogens in the adjacent electron-rich and electron-deficient units affect the shape of the backbone.[44,100]

First, we will consider the eD copolymers. Based on their OT-ωB97X-D-optimized (see Tables S1 and S2† for the OT ω values) GS trimer geometries, **BDT-TzBI**, **DTB-EF-T**, and **BDB-T-2F** have twisted backbones with different curvatures (Table 1 and Fig. 3). The backbones of **BDT-TzBI** and **BDB-T-2F** have sine wave patterns, whereas that of **DTB-EF-T** has a zigzag pattern.[101]

Table 1 Energetically the most stable conformations, backbone types, and planarity of the backbones of the studied eD and eA compounds[a] calculated at the OT-ωB97X-D/6-31G** level of theory in different environments. The dihedral angles[b] for the eD and eA compounds calculated in blend

							Dihedral angle[b] (°)			
Type	Compound	n^c	N^d	Conformation	Backbone type	Planarity	α_1	α_2	α_3	$\theta_{CRU-CRU}$[e]
eD	**BDT-TzBI**	3	30	*Anti–syn/anti*	Sine wave	Twisted	157–159	41–42	43–44	159–162
	DTB-EF-T	3	30	*Anti/syn*	Zigzag	Twisted	159–162	159–160	131–152	45
	BDB-T-2F	3	30	*Anti–syn/anti*	Sine wave	Twisted	156–162	39–44	43–44	175–178
eA	**NDI2OD-T2**	4	28	*Syn–anti/syn*	Helical	Twisted	56–57	152–153	—	60–61
	ITIC	—	—	*Anti*	Linear	Planar	180	—	—	—
	ITIC-4F	—	—	*Anti*	Linear	Planar	180	—	—	—
	ITIC-2Cl	—	—	*Anti*	Linear	Planar	180	—	—	—

[a] The neutral GS geometries. [b] See Fig. S1 and S2 for the definition of the dihedral angles. The dihedral angles of the eD and eA compounds determined in vacuum and $CHCl_3$ are presented in Table S3. [c] Number of the CRUs in the studied oligomer. [d] Number of the double bonds in the studied oligomer. [e] Between the CRUs in the oligomers.

Furthermore, the curvature of the backbone increases in the order of **DTB-EF-T** < **BDT-TzBI** < **BDB-T-2F**, which can impact the degrees of ordering and folding of the copolymer chains and the mixing of the eD and eA compounds in the blends.[97] The backbones of the eD trimers are predicted to have similar torsional twists of 2–49° from planarity regardless of the surrounding medium (Table 1 and Fig. 3; see also Table S3 and Fig. S1† for the PES curves). In all cases, each BDT donor unit and its neighboring thiophene spacers are *anti* to each other in the eD trimer models due to the repulsive S···S interactions.[99] The thiophenes and acceptor units are *syn* to each other in **BDT-TzBI** and **BDB-T-2F** because of the possible nontraditional hydrogen bonding[99] between the carbonyl oxygen of the acceptor unit and the C–H hydrogen of the neighboring thiophene. In **DTB-EF-T**, the thiophenes are *anti* to each other, except for those between the adjacent CRUs that are *syn* to each other due to a possible hydrogen bonding between the hydrogen of the unsubstituted thiophene and the carbonyl oxygen of the ester group in the thiophene of the next CRU. The same conformation has been also predicted for the dimer model of **PDTB-EF-T** in the original study of Li *et al.*[29]

Next, we will turn our attention to the eA compounds. The OT-ωB97X-D functional predicts that the eA tetramer **NDI2OD-T2** has a slightly helical backbone with a small curvature most probably due to the *syn–anti/syn* conformation (see below). The thiophene donors are predicted to be *anti* to each other with the torsion from planarity of *ca.* 27–28° between them (see Tables 1 and S3†), which is in line with, although somewhat smaller than the previous findings (the torsion of 32° from planarity by B3LYP/6-311G**[102]). The thiophene donor and NDI acceptor

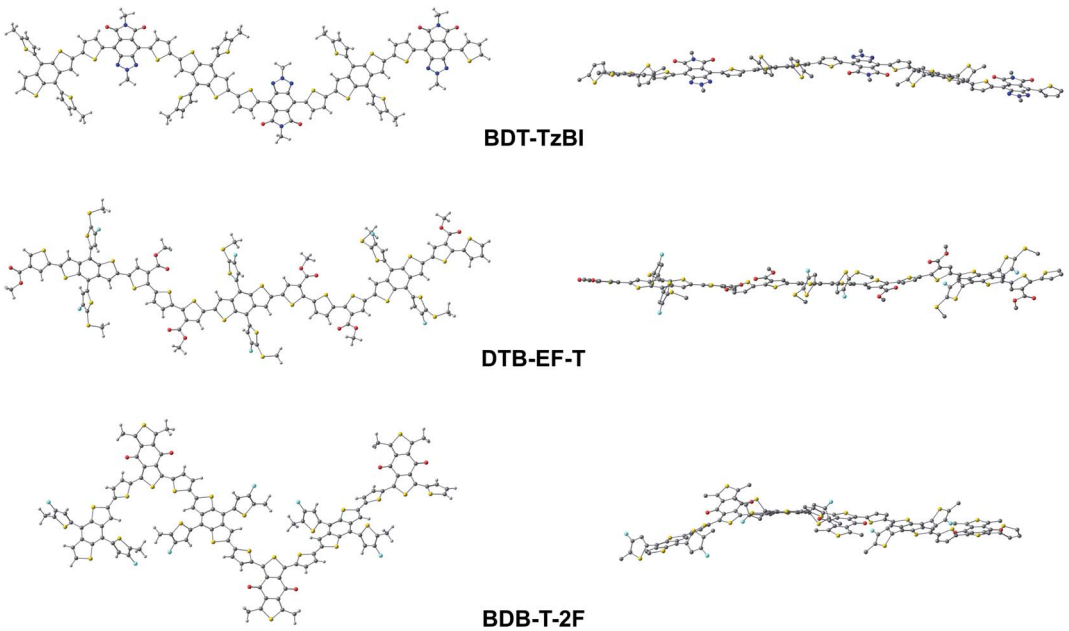

Fig. 3 Optimized GS geometries of the trimers of the studied eD copolymers calculated at the OT-ωB97X-D/6-31G** level of theory (in blend). In the side-view figures (on the right), the hydrogens are not shown for the clarity.

units of **NDI2OD-T2** are not in the same plane due to the relatively large dihedral angles (*ca.* 60°) between them (Tables 1, S3, Fig. 4 and S2†). Similar, although somewhat smaller dihedrals have been predicted previously theoretically (*syn*-conformation: 42° and *anti*-conformation: 138°) using the global hybrid functional B3LYP (with the 6-311G** basis set) and experimentally (*syn*: 37° and *anti*: 142°) with the IR and reflection–absorption IR spectroscopy measurements.[102] Here, the use of a LRC functional and truncated side groups could explain, respectively, the differences compared to the previous theoretical and experimental results.[102] Larger (*ca.* 65°) than the experimental dihedrals have been obtained previously also with a (non-tuned) LRC CAM-B3LYP functional.[103] Here, the adjacent NDI acceptor and thiophene donor units in **NDI2OD-T2** are predicted to be *syn* to each other, *i.e.* the sulfur atoms of the thiophene donors and the closest carbonyl oxygens of the neighboring acceptor units are on the same side. Previous theoretical studies have predicted varying results for the preferred orientation between the NDI and thiophenes depending on the copolymer model and functional: (i) equally stable *anti* and *syn* conformations (for the dimer model, B3LYP/6-31G*),[104] (ii) more favorable *anti* (for the monomer and pentamer models, B3LYP/6-311G**),[102] or (iii) more favorable *syn* conformation (for the dimer model, CAM-B3LYP/6-31G*).[103] Furthermore, the inclusion of full-length side chains and presence of the other **NDI2OD-T2** chains play a role in defining the more favorable conformation in the real blend environment.[105]

The OT-LRC functional OT-ωB97X-D predicts that the backbones of the SMA compounds **ITIC**, **ITIC-4F**, and **ITIC-2Cl** are completely planar (Table 1, Fig. 4 and S2†). In the experimental X-ray diffraction analysis of **ITIC** and fluorinated **ITIC** derivatives, somewhat larger torsions (4–16°) between the IT core and the INCN end-groups have been observed for their single-crystal structures.[106] Based on our calculations, **ITIC** prefers the *syn*-conformation, where the sulfurs of the IT donor core and the carbonyl oxygens of electron-deficient INCN end-groups are on the same side. This finding is consistent with both the previous theoretical calculations carried out at the B3LYP/6-31G** level of theory[107] and experimental X-ray diffraction analysis.[106] Based on these modeling results on **ITIC** compounds, both the extended π-conjugation and planarity have been gained *via* fused sp2-hybridized rings, which agree with the experimental goals for SMAs to pursue strong light absorption and good charge mobility, respectively.[17,18]

The degree of the aromaticity and delocalization of the π-electrons in the polymers, *i.e.* π-conjugation, is described by the bond length alternation (BLA) parameter, which is defined here as the average value of the differences between adjacent single and double C–C bonds. Greater delocalization leads to equalized bond lengths and thus to the lower BLA values.[108,109] The BLA values calculated for the centermost CRUs (BLA_{middle}) of the (neutral) GS geometries of the eD trimers **BDT-TzBI**, **DTB-EF-T**, and **BDB-T-2F** are very similar (Table 2, see Table S4† for the total BLA values) indicating similar delocalization along their conjugation paths (see Fig. 5). Moreover, the BLA_{middle} of the eA tetramer **NDI2OD-2T**, which has been calculated for the innermost donor and acceptor units, is only slightly larger than those of the eD trimers. If two innermost CRUs of **NDI2OD-2T** are considered instead, the BLA_{middle} values increase somewhat. Based on the positive BLA_{middle}, these eD and eA copolymers have highly alternated single and double C–C bond patterns in their backbones (also referred to as an "aromatic" character in literature sometimes[109,110]). The environment does not seem to have

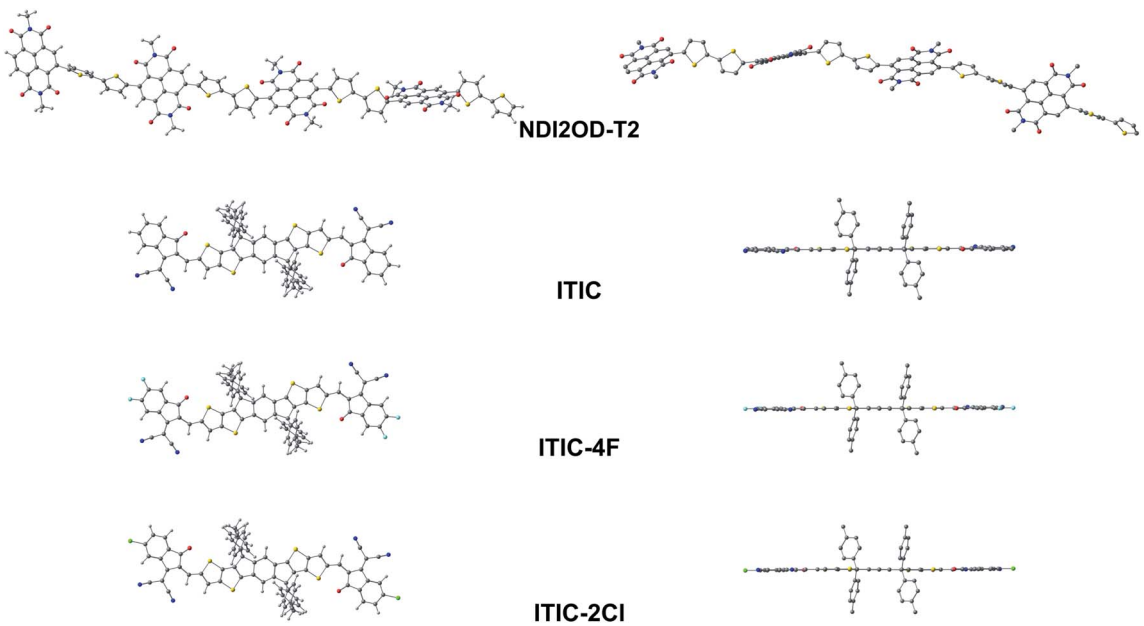

Fig. 4 Optimized GS geometries of the tetramer of the studied eA copolymer (**NDI2OD-T2**) and the SMA eA compounds (**ITIC**, **ITIC-4F**, and **ITIC-2Cl**) calculated at the OT-ωB97X-D/6-31G** level of theory (in blend). In the side-view figures (on the right), the hydrogens are not shown for the clarity.

Table 2 BLA_{middle} values[a] and intramolecular reorganization energies[b] of the studied eD and eA compounds[c] calculated at the OT-ωB97X-D/6-31G** level of theory in vacuum, $CHCl_3$ (in parentheses), and blend (in brackets)

	BLA_{middle}				Intramolecular reorganization energies	
Compound	S_0 (GS)	S_1	Cation	Anion	λ_h (eV)	λ_e (eV)
BDT-TzBI	0.046	0.006	0.016	0.017	0.30	0.42
	(0.047)	(0.000)	(0.025)	(0.021)	(0.30)	(0.44)
	[0.047]	[0.001]	[0.025]	[0.022]	[0.31]	[0.46]
DTB-EF-T	0.044	0.012[d]	0.010	0.019	0.30	0.50
	(0.045)		(0.022)	(0.023)	(0.38)	(0.60)
	[0.045]		[0.021]	[0.023]	[0.38]	[0.60]
BDB-T-2F	0.046	0.005	0.018	0.039	0.27	0.18
	(0.047)	(0.000)	(0.023)	(0.030)	(0.38)	(0.43)
	[0.047]	[0.000]	[0.041]	[0.030]	[0.42]	[0.46]
NDI2OD-T2	0.048[e]/0.051[f]	—	0.039[e]/0.029[f]	0.031[e]/0.038[f]	0.75	0.43
	(0.049[e]/0.052[f])		(0.011[e]/0.033[f])	(0.037[e]/0.046[f])	(0.64)	(0.42)
	[0.049[e]/0.052[f]]		[0.010[e]/0.032[f]]	[0.049[e]/0.052[f]]	[0.65]	[0.34]
ITIC	—	—	—	—	0.24	0.26
					(0.22)	(0.24)
					[0.22]	[0.25]
ITIC-4F	—	—	—	—	0.25	0.27
					(0.22)	(0.25)
					[0.22]	[0.25]
ITIC-2Cl	—	—	—	—	0.24	0.26
					(0.22)	(0.24)
					[0.22]	[0.24]

[a] Calculated for the conjugation paths presented in Fig. 5. [b] For the hole (λ_h) and electron transfer (λ_e). Calculated with eqn (S7) and (S8). [c] In the case of the copolymers, $n = 3$ for **BDT-TzBI**, **DTB-EF-T**, and **BDB-T-2F** and $n = 4$ for **NDI2OD-2T**. [d] The S_1 geometries of **DTB-EF-T** did not converge in either $CHCl_3$ or blend. [e] For the (three) innermost donor and acceptor units. [f] For the two innermost CRUs.

strong effect on the BLA_{middle} values, as they are very similar in blend, $CHCl_3$, and vacuum. Here we note that for molecules with a large degree of conjugation (*i.e.* long polyene and cyanine chains), the tuning of ω may lead to incorrect BLA values, which may originate from the lack of size-consistency and an unbalanced description of σ and π orbitals in the tuned LRC functionals.[111] However, as we are merely interested in the relative results between different compounds and not the absolute values, we expect the OT-LRC functional to be suitable for this case.

In conclusion, while some similar features are observed for the studied eD and eA compounds, they have distinguished features in the shapes of their backbones, degrees of the planarity, and conformational preferences, which may have impact on their packing and mixing behavior in the photoactive blends. However, we note that in the case of the copolymers, more than one backbone conformation can coexist in real solvent and solid-state environments.[105,112] Moreover, the polymer chains may adopt conformations in blends other than those predicted for single chains due to the stabilizing effects of the bulk interchain interactions.[113] The inclusion of the full-length side chains can also lead to somewhat different results compared to our models with truncated CH_3 side groups. For example, DFT PES scans of several D–A copolymers have been noted to yield more planar structures for the monomer models of CRUs than in aggregates given by MD simulations.[114] Nevertheless, these results shed more light on the intrinsic properties that may impact the interactions between the studied eD and eA compounds at their eD–eA interfaces.

Ionization of the eD and eA compounds

In the next paragraphs, we compare the ionization (both the oxidation and reduction) characteristics of the studied eD and eA compounds. In general, oxidation and reduction cause notable changes in the geometries of the eD and eA oligomers, as is observed from the bond length differences (Fig. 5 for blend and Fig. S4† for vacuum and $CHCl_3$) and the BLA values (Tables 2 and S4†) of the radicals (cation and anion) with respect to the corresponding neutral compounds. The largest changes in the eD and eA oligomers caused by oxidation and reduction occur mainly in their middle regions, *i.e.* the centermost CRUs, although there are some variations depending on the surrounding medium. Moreover, larger intramolecular reorganization energies for the hole (λ_h) and electron (λ_e) transfer, which correspond to the relaxation energies of the compounds upon oxidation and reduction, respectively, are predicted in blend and $CHCl_3$ indicating somewhat larger geometrical changes in these environments compared to vacuum (Table 2). Ionization of the neutral oligomers mainly shortens the single bonds and lengthens the double bonds resulting in an inverse single–double C–C bond pattern compared to the neutral GS geometries. Decreased bond length alternation between single and double bonds and thus increased delocalization can be observed also from smaller BLA_{middle} values of the most radicals compared to the neutral compounds (Table 2).

Oxidation induces rather similar geometrical changes to all three eD trimer models, as can be observed from their bond length difference patterns (Fig. 5 and S4†). However, the

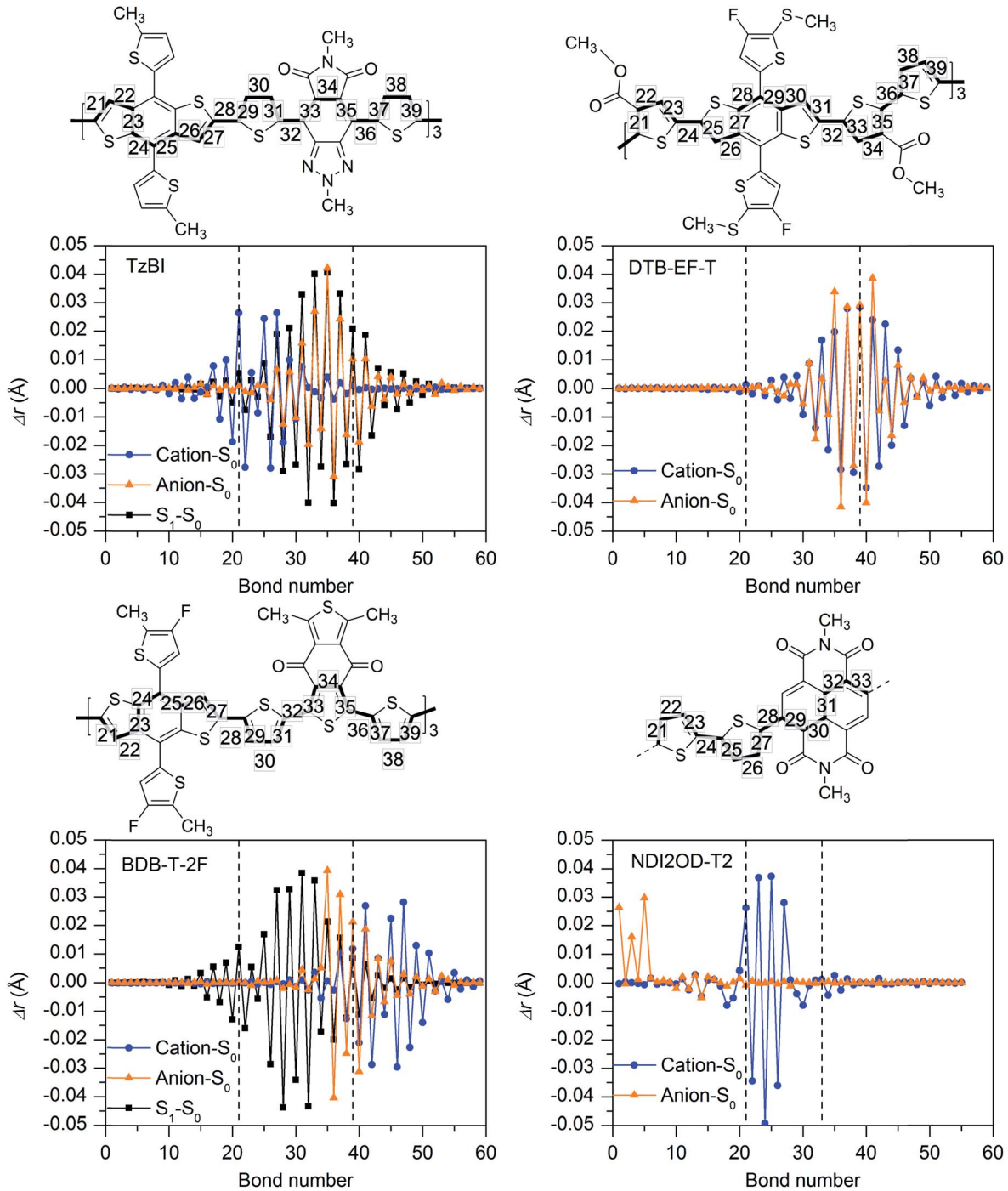

Fig. 5 Differences in the bond lengths (Δr) between the OT-ωB97X-D/6-31**-optimized (in blend) geometries of charged (radical cation, radical anion, or S_1) and neutral (GS) compounds with respect to the bond numbers of the eD and eA compounds along the conjugation paths presented above the graphs. The numbering in the chemical structures corresponds to the middle CRUs, which are represented with the dashed lines in the graphs. As **NDI2OD-T2** is the tetramer, three centermost units are considered for it instead of the middle CRUs.

backbone regions, which are affected the most by oxidation, are somewhat different for them. In **BDT-TzBI** and **BDB-T-2F**, the largest changes are observed in both the BDT donor and thiophene spacer units, whereas in **DTB-EF-T**, the largest changes caused by oxidation take place in both the unsubstituted electron-rich and ester-substituted electron-deficient thiophenes (see 'Excited-state characteristics of the isolated eD and eA compounds' below), while the BDT donor units are mainly unaffected. The λ_h values (Table 2) and IEs (both VIEs and AIEs, Fig. S5 and Table S5 in ESI†) of the eD trimers increase slightly in the order of **BDT-TzBI** < **DTB-EF-T** ≤ **BDB-T-2F** in both blend and $CHCl_3$, which indicates the smallest changes for **BDT-TzBI** making it the easiest to oxidize among the studied eD trimers (in vacuum, the trends in the λ_h and IE values vary more). The

calculated λ_h values suggest that the hole mobilities of the eD compounds increase in the order of **BDB-T-2F** < **DTB-EF-T** < **BDT-TzBI**, which is in line with the experimental hole mobilities predicted for the corresponding copolymers.[28,29,115]

Reduction of the eD trimers takes mainly place in different backbone regions than oxidation, namely in the acceptor units and neighboring thiophenes for **BDT-TzBI** and **BDB-T-2F**. The surrounding medium has some effect on these regions, as reduction of **BDB-T-2F** affects mostly its thiophene spacers in vacuum instead of the BDD acceptor unit. In **DTB-EF-T**, reduction takes place in the same units as oxidation, *i.e.* the unsubstituted electron-rich and substituted electron-deficient thiophenes. The λ_e values of the eD trimers increase in the order of **BDB-T-2F** < **BDT-TzBI** < **DTB-EF-T** (in all media) following the same trend as their λ_h values in vacuum (Table 2). Overall, the λ_h values are predicted to be smaller than the λ_e values for the eD compounds indicating faster hole mobilities,[43] as can be expected from their nature as the hole-transporting materials.[103]

Similar trends in ionization are observed for the eA tetramer **NDI2OD-T2** as for the eD trimers **BDT-TzBI** and **BDB-T-2F** in all media, namely the oxidation of **NDI2OD-T2** takes place in the electron-rich thiophene donor units, whereas the reduction affects mostly the NDI acceptor unit and some of the thiophenes. However, larger geometrical changes take place in **NDI2OD-2T** upon oxidation compared to the other eD and eA compounds, as can be concluded from the bond length difference patterns (Fig. 5 and S4†) and the larger λ_h values of **NDI2OD-2T** (Table 2). This is most probably due to the two neighboring, unsubstituted thiophene donor units within the CRU of **NDI2OD-2T**, which introduce more flexibility and degrees of freedom to the backbone compared to the more conjugated donor units in the other eD and eA compounds. On the contrary, reduction induces only small changes to the more rigid NDI acceptor unit of **NDI2OD-T2**, as can be observed from the bond length differences (predicted in all media) and the λ_e value (predicted in blend). Overall, the calculated reorganization energies are consistent with the previously predicted λ_h (0.38–0.56 eV [103,116]) and λ_e (0.30 eV [103]) values for the oligomers (n = 1–5) of **P(NDI2OD-2T)** with the (non-tuned) LRC CAM-B3LYP functional. The smaller λ_e values of **NDI2OD-2T** compared to its λ_h values indicate faster electron mobility than the hole mobility, as expected from its electron-transporting nature.

Based on their somewhat smaller λ_h and λ_e values, the geometrical changes upon oxidation and reduction in the eA **ITIC** derivatives are not as large as in the eD and eA copolymer

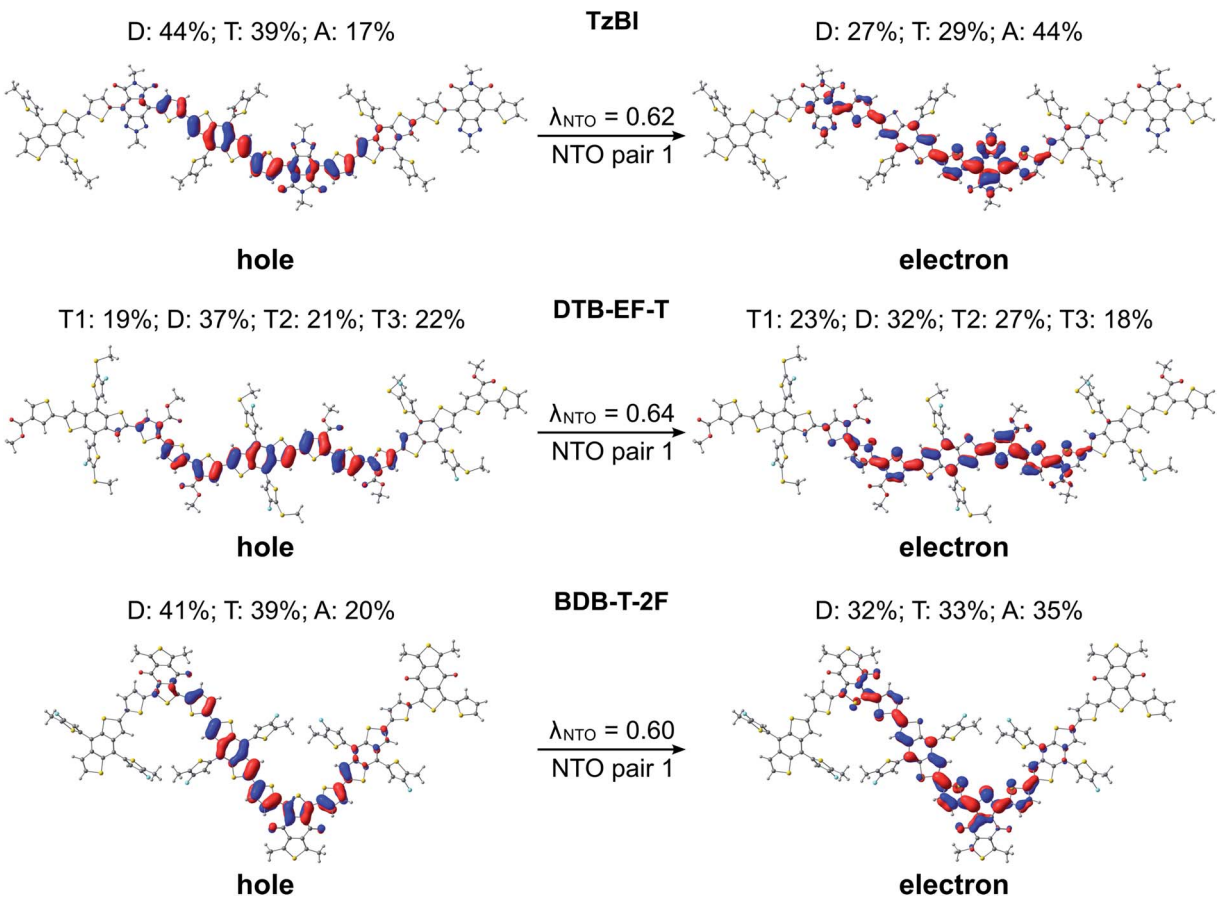

Fig. 6 NTOs (the dominant pairs) for the main excitations (*i.e.* $S_0 \rightarrow S_1$ transitions) of the studied eD compounds calculated with TDDFT at the OT-ωB97X-D/6-31G** level of theory in blend (isodensity contour = 0.025). Additionally, the contributions (%) of the electron densities of donor (D), acceptor (A), and thiophene (T) units of the oligomers to the NTOs and the fraction of each NTO pair (λ_{NTO}) related to the $S_0 \rightarrow S_1$ transition are presented.

models. In addition, the λ_h and λ_e values of **ITIC** derivatives are almost identical with each other despite the different substituents in their electron-withdrawing INCN end-groups. The smaller λ_h and λ_e values are not surprising,[43,117] as one aim of the rigid A–D–A type backbones of the **ITIC**-based compounds has been to reduce their reorganization energies for improved charge transport. In comparison, the studied eD and eA oligomers have more flexibility and degrees of freedom between their backbone units, which lead to the larger reorganization energies for the hole and electron transfer.

Excited-state characteristics of the isolated eD and eA compounds

Next, we turn our attention to the excitation characteristics of the studied NF PSC compounds. First, the intramolecular CT characters of the eD and eA compounds will be compared by examing the NTOs of their main transitions, *i.e.* those with the largest oscillator strengths corresponding to the absorption maxima in their calculated UV-vis spectra (Fig. S6 and Table S6†). In the eD and eA oligomers (*i.e.* trimers for eDs and tetramer for the eA copolymer), both the hole and electron NTO determined in blend are mainly localized in the middle CRU (or CRUs, see Fig. 6 and 7). The surrounding medium does not have much effect on the charge distribution, and the NTOs predicted in vacuum and $CHCl_3$ are almost the same (see Table S7†) and thus are not presented here.

In all compounds, a partial intramolecular CT is observed from the electron-rich donor units to the electron-deficient acceptor units, as expected.[17,18,65,100,118] In the eD trimers, charge transfers also from the thiophene spacers to the acceptor units, namely the hole NTOs are more localized on the donor and thiophene units, whereas the electron NTOs are more localized on the acceptor units. This contribution of the thiophenes to the CT is in line with their known, weakening effect on the push–pull interaction between the donor and acceptor units.[37] The nature of CT is rather similar in **BDT-TzBI** and **BDB-T-2F**, which have the same electron-rich units, *i.e.* the BDT donor and thiophene spacer units, but different acceptor units. However, a somewhat larger amount of charge density moves from the electron-rich units to the acceptor unit in the case of **BDT-TzBI** compared to **BDB-T-2F** (TzBI: 31 percentage points, *i.e.* pp, *vs.* **BDB-T-2F**: 16 pp, see Table S7†). We predicted also in our previous study[65] a similar kind of CT character for a copolymer with a similar backbone structure, where the BDT donor unit and the quinoxaline acceptor unit were separated by the thiophene spacers. As the corresponding eD copolymers have been incorporated in the efficient fullerene-based and NF PSCs, this kind of a backbone structure and resulting CT character can be concluded to be beneficial for the performance of the

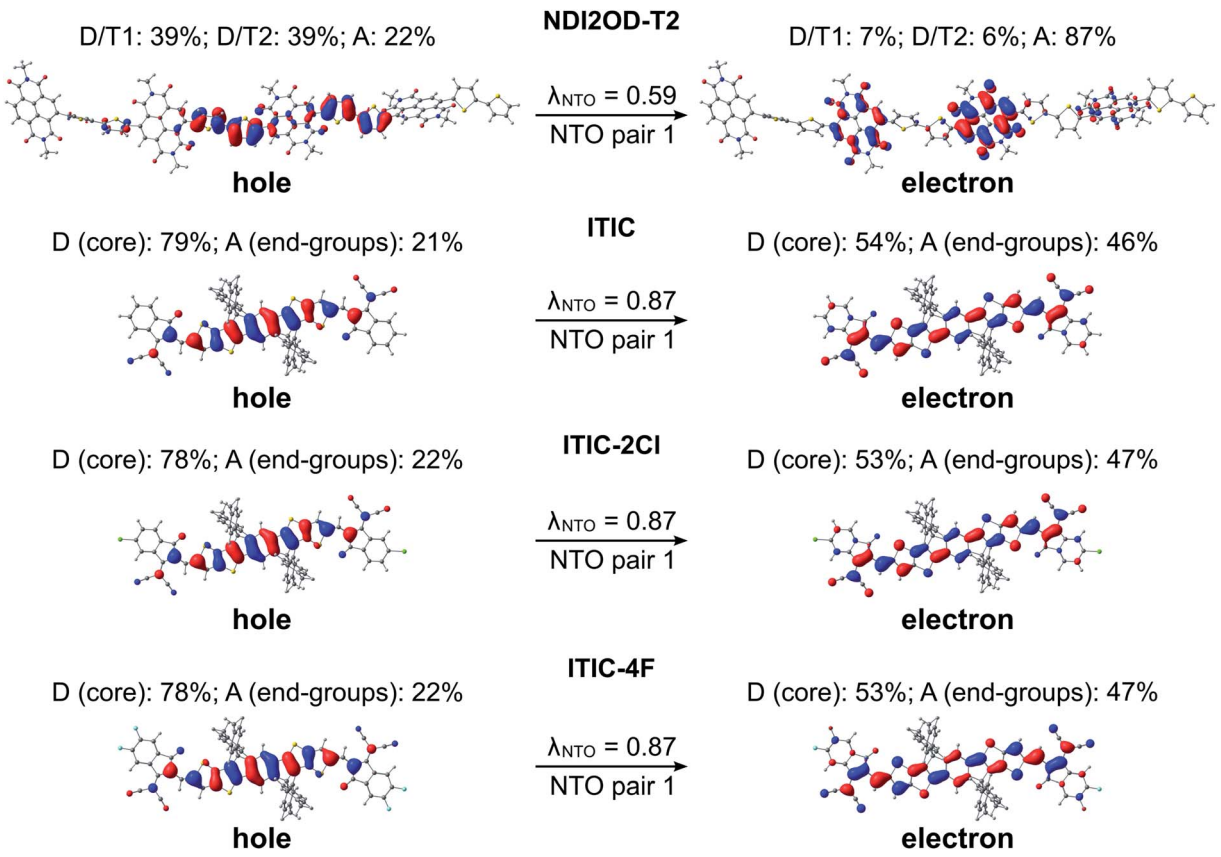

Fig. 7 NTOs (the dominant pair) for the main excitations (*i.e.* $S_0 \rightarrow S_1$ transitions) of the studied eA compounds calculated with TDDFT at the OT-ωB97X-D/6-31G** level of theory in blend (isodensity contour = 0.025). Additionally, the contributions (%) of the electron densities of the donor (D) and acceptor (A) units of the compounds to the NTOs and the λ_{NTO} values are also presented.

PSCs. However, no exact conclusion on the efficiencies can be drawn merely based on these factors. Namely, **DTB-EF-T**, whose corresponding copolymer has been employed in the highly efficient NF PSC, has somewhat different backbone structure and intramolecular CT characteristics. In **DTB-EF-T**, both the hole and electron NTOs are quite evenly distributed along the BDT donor and thiophene units and only a small amount of charge (*ca.* 9 pp) is transferred from the BDT donor units and unsubstituted thiophenes to the electron-deficient thiophenes with the ester side groups.

In the eA tetramer **NDI2OD-T2** (Fig. 7), the hole NTOs are more clearly localized on the thiophene donor units and the electron NTOs on the NDI acceptor units compared to the NTOs in the eD trimers, which are more delocalized along several donor and acceptor units (see Fig. 6). This is most probably due to the larger twists between the donor and acceptor units in **NDI2OD-T2** compared to the eD trimers (see Table 1) hindering the delocalization along the backbone.

For all three **ITIC**-based SMAs, the hole NTO is more localized on the electron-donating IT core group, whereas the electron NTO is quite evenly distributed on both the core and electron-withdrawing INCN end-groups (Fig. 7). Fluorination and chlorination of the INCN end-groups have been stated to enhance the intramolecular CT nature of **ITIC**, as based on the larger dipole moments predicted for the halogenated regional parts.[33] However, the introduction of either F or Cl atoms did not affect the electron density distributions of the highest occupied molecular orbital (HOMO) and lowest unoccupied molecular orbital (LUMO). The same is observed here with the NTOs, which are also very similar to each other indicating that the fluorination and chlorination does not affect the electron density distribution much in these models. However, slightly smaller vertical excitation energies of the main, $S_0 \rightarrow S_1$ transition (Table S6†) and consequently red-shifted UV-vis spectra of **ITIC-4F** and **ITIC-2Cl** (Fig. S6†) indicate some enhancement in their intramolecular CT character with respect to **ITIC**, which is in line with the experimentally predicted UV-vis absorption spectra.[33]

Next, we compare the GS and S_1 state geometries of the eD trimers to display the structural changes taking place upon the excitation and resulting vibrational relaxation. The S_1 relaxation energies increase from those calculated for **BDT-TzBI** (210 kJ mol^{-1} in vacuum; 204 kJ mol^{-1} in $CHCl_3$; 205 kJ mol^{-1} in blend) and **DTB-EF-T** (217 kJ mol^{-1} in vacuum) to those for **BDB-T-2F** (221 kJ mol^{-1} in vacuum; 213 kJ mol^{-1} in $CHCl_3$; 214 kJ mol^{-1} in blend). Smaller relaxation energies indicate smaller geometrical changes in **BDT-TzBI** than in the other two eD trimers upon excitation. These trends are similar as those of the λ_h values calculated in $CHCl_3$ and blend (see above, Table 2). The BLA_{middle} values for the optimized S_1 geometries of the eD **BDT-TzBI** and **BDB-T-2F** trimers are practically zero in all media indicating highly delocalized structures (Table 2). The BLA_{middle} value of **DTB-EF-T** (in vacuum) is also notable smaller due to more delocalized backbone compared to the neutral GS geometry. The largest differences in the bond lengths between the GS and S_1 state geometries of the eD trimers are mainly in the acceptor and neighboring thiophene units of the middle CRU, *i.e.* in the same regions as for reduction (Fig. 5 and S4†). However, small structural changes occur in the BDT donor of BTB-T-2F, as well, which might explain its larger S_1 relaxation energies.

Local interfacial eD–eA configurations

After establishing the structural and optoelectronic features of the individual eD and eA compounds, we will focus next on the eD–eA complexes and their structural and CT characteristics to better understand the interactions at their local eD–eA interfaces. In the case of the polymer–polymer system **BDT-TzBI–NDI2OD-T2**, the most stable configuration is predicted to form when the NDI acceptor units of **NDI2OD-T2** ($n = 1$) and **BDT-TzBI** ($n = 1$) are face-to-face, while their donor units are also face-to-face (the AA(1) configuration, see Tables S8–S10† and Fig. 8 and S7†). In another possible configuration (*i.e.* the DA(2) configuration with the energy difference of 0.9 kJ mol^{-1} compared to the most stable one), the acceptor unit of **NDI2OD-T2** and the donor units of **BDT-TzBI** are face-to-face, while the donor units of **NDI2OD-T2** and the acceptor unit of **BDT-TzBI** are face-to-face. This agrees with the experimental evidence[119] for the face-to-face stacking between the similar PTzBI-Si copolymer and **P(NDI2OD-T2)**. These kinds of face-to-face orientations are essential for forming strong π-orbital overlap at the polymer–polymer interfaces, reducing the binding energy of the excitons, and promoting the formation of free charge carriers.[37] The calculated distances between the backbones of **BDT-TzBI** and **NDI2OD-T2** are *ca.* 3.4–4.0 Å with the average of 3.7 Å, which is consistent with the experimental π–π distance (3.7 Å).[120] Based on the electrostatic potential energy surface maps (Table S11†) calculated for the different configurations of **BDT-TzBI–NDI2OD-T2**, there are subtle differences in the electronegative and electropositive regions, which could have roles in defining the energetically favorable positioning of **BDT-TzBI** and **NDI2OD-T2** observed in the studied set of configurations.

In the case of the polymer–SMA systems, energetically favored placement of the eA SMA compound above the eD copolymer compounds depends on the system. Namely, for **DTB-EF-T–ITIC-4F**, the most stable configuration is predicted to be the one where the electron-withdrawing end-group of **ITIC-4F** is on the top of the BDT donor unit of **DTB-EF-T** (the DA configuration, see Table S9†). Even in the model, where the end-group of **ITIC-4F** has been initially positioned on the top of the acceptor (the AA configuration) **ITIC-4F** has shifted so that the end-group is located above the bond connecting the acceptor and donor units of **DTB-EF-T**. However, in **BDB-T-2F–ITIC-2Cl**, energetically the most favorable configuration is the one where the end-group of **ITIC-2Cl** is on the top of the BDD acceptor unit of **BDB-T-2F** (the AA configuration, see Table S10†). This is consistent with the previous atomistic simulations of the **BDB-T-2F–ITIC** systems,[49,121] where the end-groups of **ITIC** are observed to locate more probably on the top of the acceptor unit than the donor unit of **BDB-T-2F**.

We note that our models of the monomers with the truncated side groups cannot entirely describe the best possible arrangements of the studied compounds, as the full side chains

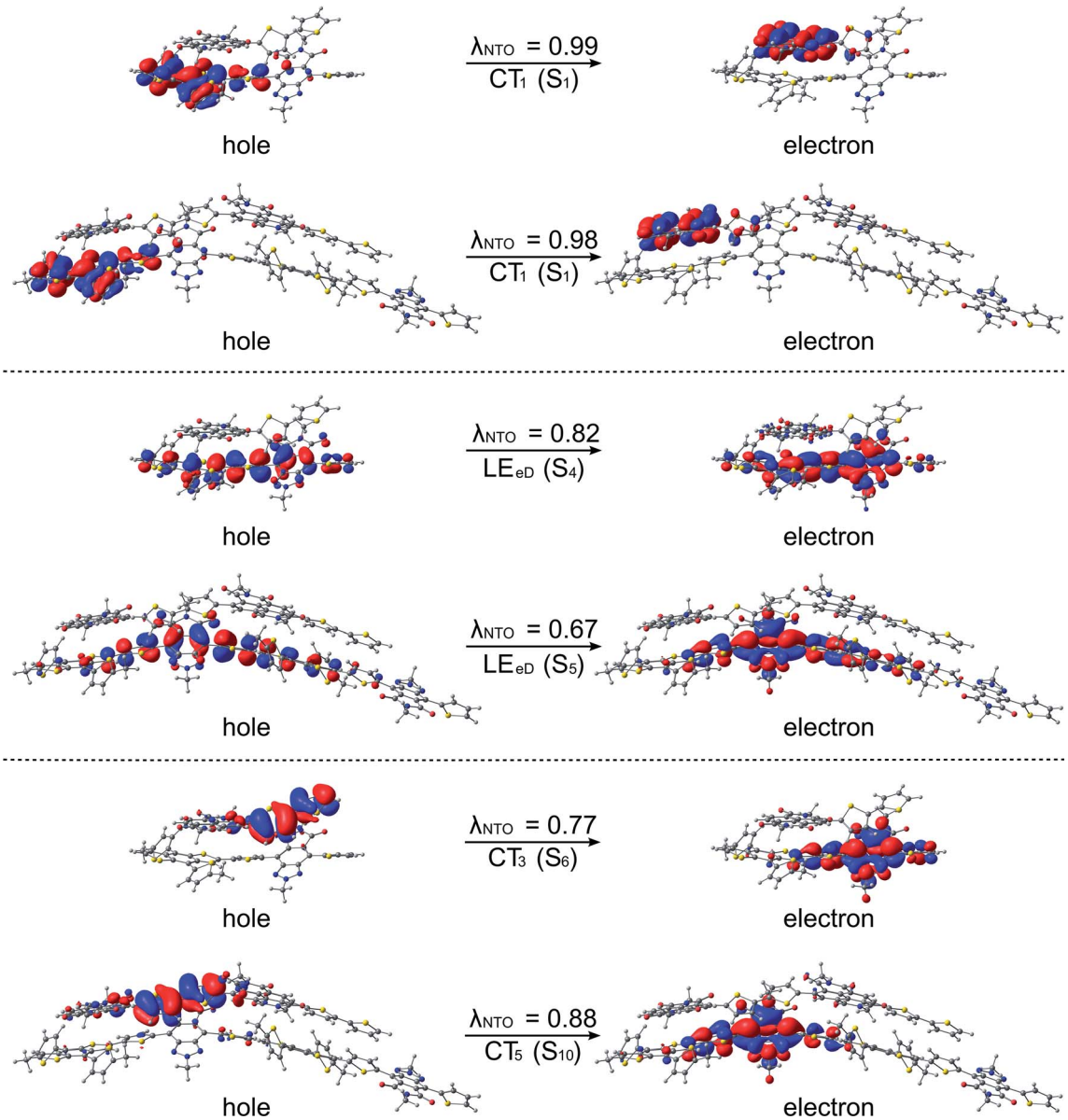

Fig. 8 NTOs (the dominant pairs) for the CT and LE states of the **BDT-TzBI–NDI2OD-T2** complexes (the DA(2) configurations) calculated with TDDFT at the OT-ωB97X-D/6-31G** level of theory in blend. The complexes have been constructed using either the monomer or dimer models of both **PBDT-TzBI** and **P(NDI2OD-T2)**. Additionally, the λ_{NTO} values are also presented.

will most likely set steric hindrances in some configurations and prevent the compounds getting as close as in the monomer-based complexes studied here. Additionally, the single CRU models (monomers) do not take the effects that the additional CRUs might have on the preferred relative positioning in the copolymer backbone into account. Thus, we optimized the geometry of **BDT-TzBI–NDI2OD-T2** also by using the dimers of **PBDT-TzBI** and **P(NDI2OD-T2)** for the DA(2) configuration, for comparison (see Table S8† and Fig. 8). The relative positions of **BDT-TzBI** and **NDI2OD-T2** in the dimer configuration are rather similar as in the monomer configuration, indicating that the sizes of the D–A oligomers do not seem to have a significant effect at least not for this system. More importantly, the predicted CT characteristics in complexes are very similar for both the monomer and dimer models (see 'Charge transfer characteristics in the local interfacial eD–eA complexes' below). Unfortunately, the geometry optimization of the DA(2) dimer configuration was computationally so demanding that we were unable to verify the effect of size for the other systems. Thus, even though our truncated models may introduce some inaccuracies to the results, our models can give some insight into the relative placements of the studied eD and eA compounds and the CT characteristics at their local interfaces.

Charge transfer characteristics in the local interfacial eD–eA complexes

Next, the nature of the excited states relevant to the ED and CR processes of the eD–eA complexes will be examined. The most

stable configurations of the interfacial eD–eA complexes will be investigated in the case of the polymer–SMA systems. For the polymer–polymer **BDT-TzBI–NDI2OD-T2** system, the DA(2) configuration will be discussed instead due to its larger electronic couplings and CT rates compared to the most stable AA(1) configuration (see "Calculating the CT rates for the local interfacial eD–eA complexes" below). In the DA(2) configuration of **BDT-TzBI–NDI2OD-T2**, the S_1 state is the CT_1 state, where the hole NTO is delocalized on the BDT donor and thiophene units of **BDT-TzBI** and the electron NTO is localized on the NDI acceptor unit of **NDI2OD-T2** (Fig. 8). In other words, the charge transfers from the electron-rich units of **BDT-TzBI** to the electron-deficient unit of **NDI2OD-T2**. The LE state, which is the local excitation of the eD compound, **BDT-TzBI**, is predicted to be higher in energy (*i.e.* the S_4 state here) than the CT_1 state. An opposite ordering of the LE and CT_1 states is sometimes detected for the copolymer–$PC_{71}BM$ complexes with both the non-tuned LRC and OT LRC functionals.[65,66] Interestingly, in the third lowest CT state, *i.e.* CT_3, CT is observed from the eA compound **NDI2OD-T2** to the eD compound **BDT-TzBI**. Namely, the charge transfers from the thiophene donor units of **NDI2OD-T2** to several units of **BDT-TzBI**, the largest amount of the electron NTO being on the TzBI acceptor unit. This kind of a CT could originate from the hole transfer from the eA compound to eD, also referred to as the "Channel II" CT process, which may participate in the regular electron transfer process from the eD compound to eA in charge generation of APSCs.[37,122]

As mentioned above (see "Local interfacial eD–eA configurations"), the use of longer oligomers for constructing the complexes would have been more ideal instead of the truncated monomer models. However, when comparing the NTOs of the monomer and dimer models of the DA(2) configuration of **BDT-TzBI–NDI2OD-T2**, it can be observed that the nature of the CT processes is rather similar in both models (Fig. 8). Moreover, the ordering of the states is the same, namely the CT_1 state is below both the LE state and the CT state (CT_5 for the dimer model, CT_3 for the monomer model), where the CT occurs from the eA compound to the eD compound. For both the monomer and dimer configurations, the hole and electron NTOs of the CT states are localized in the equally large regions regardless the sizes of the eD and eA models. The LE state, while having the same shape in both the monomer and dimer configurations, is not distributed only on a single CRU but on the both CRUs in the dimer configuration. To conclude, as both the monomer and dimer models have very similar charge distributions, the smaller monomer models can be expected to provide sufficiently good description of the nature of the states for this NF PSC system.

The relative positioning of **BDT-TzBI** and **NDI2OD-T2** has some effect on the nature of the states, although the overall shapes of the NTOs are rather similar. Namely, in the AA(1) configuration (Fig. S7†), the hole NTO of CT_1 and the electron NTO of CT_3 are more delocalized along the whole backbone of **BDT-TzBI** compared to the DA(2) configuration (Fig. 8). Moreover, a small amount of a local excitation of the eA compound **NDI2OD-T2** is mixed with the CT_1 state in the AA(1) configuration. We have observed the similar mixing of the local and CT states also for different copolymer–$PC_{71}BM$ complexes in our previous theoretical studies.[65,66] This is due to the tendency of the LRC functionals to predict the mixed states for these kinds of photoactive systems. The absence of the local excitations in the CT state of the DA(2) configuration might explain its faster ED and CR rates compared to the AA(1) configuration (see Table 3 and Fig. 11). However, previous experimental[123] and theoretical[51,123] studies have also speculated that the delocalized CT states at the eD–eA interfaces of organic solar cells could be beneficial for decreasing the Coulomb binding energy as a result of reduced electrostatic attraction between the hole and electron.

The studied polymer–SMA systems exhibit the same ordering of the states as the polymer–polymer system **BDT-TzBI–NDI2OD-T2**, *i.e.* the CT_1 (S_2) is at a lower energy than the LE state (S_7 for **DTB-EF-T–ITIC-4F** and S_4 for **BDB-T-2F–ITIC-2Cl**, Fig. 9 and 10). In both **DTB-EF-T–ITIC-4F** and **BDB-T-2F–ITIC-2Cl**, the natures of the CT_1 states are quite similar and CT occurs from the eD compound, *i.e.* **DTB-EF-T** and **BDB-T-2F**, to the end-group of the **ITIC**-based eA compound, *i.e.* **ITIC-4F** and **ITIC-2Cl**, respectively. In the both polymer–SMA systems, the hole NTO of the CT_1 state is distributed over several backbone units of the eD compounds, although in **DTB-EF-T**, the charge density is more localized on the donor unit, whereas in **BDB-T-**

Table 3 Charge transfer rate parameters[a] for the ED and CR processes for the selected configurations of the eD–eA complexes[b] calculated at the OT-ωB97X-D/6-31G** level of theory in blend

Complex	Configuration	$H_{if,ED}$ (meV)	$H_{if,CR}$ (meV)	$\lambda_{i,ED}$ (eV)	$\lambda_{i,CR}$ (eV)	ΔG°_{ED} (eV)	ΔG°_{CR} (eV)	k_{ED}[c] (s^{-1})	k_{CR}[c] (s^{-1})
BDT-TzBI–NDI2OD-T2	DA(2)	37.54	72.74	0.43	0.30	−0.81	−1.70	1.92×10^{13}	9.78×10^{9}
	AA(1)	16.55	47.76	0.43	0.32	−0.68	−1.81	2.12×10^{12}	1.13×10^{9}
DTB-EF-T–ITIC-4F	DA	110.91	99.80	0.22	0.30	−0.56	−2.03	1.52×10^{14}	5.83×10^{6}
	AA	0.35	24.38	0.23	0.32	−0.59	−2.01	1.65×10^{9}	1.70×10^{6}
BDB-T-2F–ITIC-2Cl	DA	6.87	70.37	0.28	0.24	−0.36	−2.00	1.77×10^{12}	3.18×10^{5}
	AA	33.82	131.83	0.32	0.30	−0.50	−1.83	5.05×10^{12}	1.72×10^{9}

[a] Electronic couplings (H_{if}) calculated with the multi-state (11 states) FCD scheme (eqn (S22)–(S24)), inner (intermolecular) reorganization energies (λ_i, eqn (S10)–(S15)), Gibbs free energies (ΔG°, eqn (S16)–(S19)), and CT rates (k, eqn (1)). The Coulomb energies (eqn (S17) and (S19)) are presented in Table S15. [b] See Table S16 for the parameters and rates for the other configurations of **BDT-TzBI–NDI2OD-T2**. [c] The rates presented in this table were calculated using the external reorganization energy of 0.53 eV, chosen from the range of the possible values shown in Fig. 11.

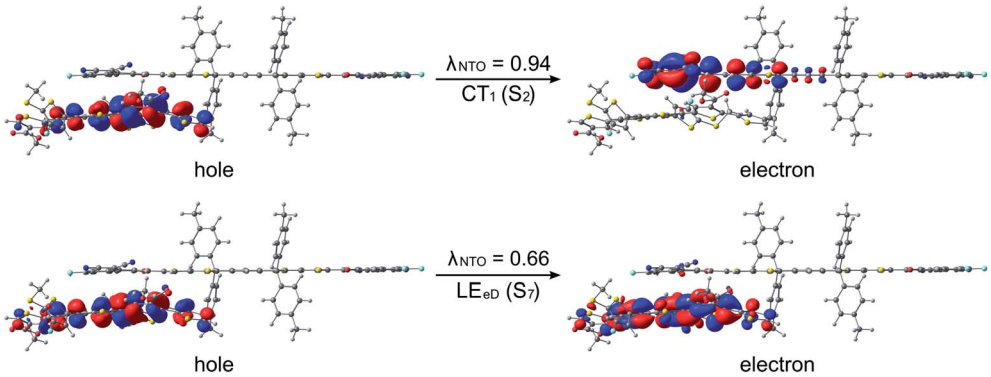

Fig. 9 NTOs (the dominant pairs) for the CT_1 and LE states of the **DTB-EF-T–ITIC-4F** complex (the DA configuration) calculated with TDDFT at the OT-ωB97X-D/6-31G** level of theory in blend. Additionally, the λ_{NTO} values are also presented.

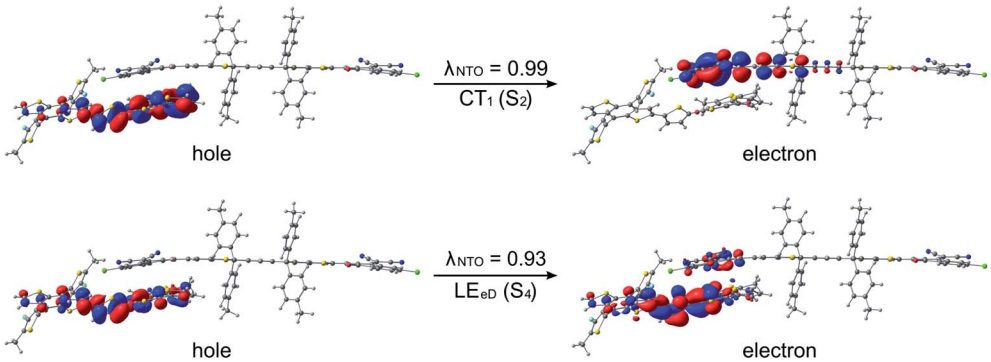

Fig. 10 NTOs (the dominant pairs) for the CT_1 and LE states of the **BDB-T-2F–ITIC-2Cl** complex (the AA configuration) calculated with TDDFT at the OT-ωB97X-D/6-31G** level of theory in blend. Additionally, the λ_{NTO} values are also presented.

2F, it mainly localizes on the acceptor unit. Here, no CT from the eA **ITIC** compounds to the eD monomers were observed for the polymer–SMA systems, although there have been experimental evidence for the "Channel II" process also in several polymer–SMA systems.[124] However, only the 10 lowest excited singlet states have been considered here, so it is possible that this type of a "Channel II" CT could be observed at higher-energy states.

Calculating the CT rates for the local interfacial eD–eA complexes

Finally, we have calculated the CT rate parameters and rates for the ED and CR processes (Tables 3 and S12–S16). First, we will consider the electronic couplings, which, as expected, are highly sensitive to the relative positions of the eD and eA compounds.[66,125–128] Overall, the largest couplings are predicted mainly for the most stable polymer–SMA systems, *i.e.* the DA and AA configurations of **DTB-EF-T–ITIC-4F** and **BDB-T-2F–ITIC-2Cl**, respectively (see Tables 3, S12, and S13†). In the **BDT-TzBI–NDI2OD-T2** polymer–polymer system, the second most stable DA(2) configuration has somewhat stronger couplings than the most stable AA(1) configuration; the energy difference between the configurations is 0.9 kJ mol^{-1}. The CR couplings are predicted to be larger than the ED couplings in all the other systems, except in the DA configuration of **DTB-EF-T–ITIC-4F**. We observed larger CR couplings compared to ED couplings also previously in our study of the copolymer–fullerene system.[66]

Next, we will discuss the effect of the dispersion corrected OT-LRC functional on calculating the electronic couplings for different NF PSC systems with the two- and multi-state FCD schemes in complement to our previous study[66] of the multi-state electronic couplings of polymer–fullerene PSC system. In that case, both the non-tuned CAM-B3LYP and OT-BNL LRC functionals predicted oscillating coupling values especially for the CR couplings of the TQ–$PC_{71}BM$ complexes with the increasing number of the states.[66] On the contrary, both the ED and CR couplings predicted here for the polymer–polymer **BDT-TzBI–NDI2OD-T2** are relatively constant with different number of states (2–26, Table S12†). Similar trends, *i.e.* consistent two- and multi (11)-state electronic couplings, are also predicted for the polymer–SMA systems (Table S13†), although in their case the effect of the larger number of states could not be confirmed due to the convergence problems in computations. Here, we have only carried out the calculations with the dispersion corrections and with tuning the default value of ω (*i.e.* using the optimally tuned OT-ωB97X-D functional) so we cannot determine, whether the constant couplings result from the

dispersion corrections or from the tuning of the ω. Moreover, the studied system may affect the couplings, as well. However, as the dispersion corrections are important for the correct description of the local interfacial eD-eA complexes,[65,68,69] their inclusion can be expected to be beneficial also for calculating electronic couplings in these PSC systems. Thus, while final conclusions cannot be drawn merely from these results, they are still encouraging in a sense that dispersion corrections seem to stabilize the coupling values when employed with the OT-LRC functionals.

The second important CT rate parameter is the inner (intermolecular) reorganization energy, λ_i, which describes the structural changes in the geometries of the eD and eA compounds upon CT.[126] For the efficient ED process and fast ED rates, the reorganization energy of the system should be minimized. In most cases, the λ_i (and consequently the total λ, *i.e.* $\lambda_i + \lambda_s$) values are larger for the ED process than for the CR process (Table 3) indicating that the faster ED rates with respect to the CR rates are due to the other CT parameters (see below). The λ_i values predicted for **BDB-T-2F–ITIC-2Cl** agree with those ($\lambda_{i,ED}$ of *ca.* 0.20 eV and $\lambda_{i,CR}$ of *ca.* 0.25–0.29 eV) calculated previously for the similar system of **BDB-T-2F** and methoxy-substituted **ITIC** (**ITIC**-OM) by Wang and Brédas.[49] A closer look at the contributions of the eD and eA compounds to the inner reorganization energies reveals the differences in their geometrical changes during the ED and CR processes (Table S14†). The eD trimers **BDT-TzBI** and **BDB-T-2F** are predicted to undergo larger geometric changes upon ED (*i.e.* $eD^* \rightarrow eD^+$) than CR (*i.e.* $eD^+ \rightarrow eD$), whereas the geometrical changes in **DTB-EF-T** are larger during CR than ED. In other words, for **BDT-TzBI** and **BDB-T-2F**, the geometries of the S_1 state and cation differ more than those of the cation and neutral species. The contribution of the eA compound is the same for both ED and CR, *i.e.* when going from the GS geometry to that of the radical anion ($eA \rightarrow eA^-$) and *vice versa* ($eA^- \rightarrow eA$). Overall, the $\lambda_{i,CR}$ values for the studied NF PSC systems are close to each other, whereas the $\lambda_{i,ED}$ values increase somewhat in the order of **DTB-EF-T–ITIC-4F** < **BDB-T-2F–ITIC-2Cl** < **BDT-TzBI–NDI2OD-T2**. This ordering indicates smaller geometrical relaxation upon ED for the polymer–SMA systems compared to the polymer–polymer system, which may be one factor explaining the higher efficiencies predicted for these SMA containing NF PSCs.[27,29,129]

Next, we will consider the third CT parameter, *i.e.* the Gibbs free energy for the CT reaction that is the energy difference (*i.e.* driving force) between the LE and CT_1 states for the ED process and between the CT_1 state and GS for the CR process. For the efficient ED process, the ΔG°_{ED} value should be maximized. Based on the negative values of ΔG°, both the ED and CR processes are predicted to be spontaneous in all the complexes (Table 3). The $|\Delta G^\circ_{ED}|$ values of **BDB-T-2F–ITIC-2Cl** are consistent with those (0.11–0.45 eV) predicted previously for the similar **BDB-T-2F–ITIC**-OM systems at the OT-ωB97XD/6-31G* level of theory.[49] The value of the external reorganization energy defines (the range of 0.10–0.75 eV has been considered here for λ_s, see ESI† for the justification), whether the ED processes of the studied systems take place in the Marcus normal region ($|\Delta G^\circ_{ED}| < \lambda_{ED}$, where $\lambda_{ED} = \lambda_{i,ED} + \lambda_s$). The CR processes of all the systems are predicted to occur deep in the Marcus inverted region ($|\Delta G^\circ_{CR}| \gg \lambda_{CR}$, where $\lambda_{CR} = \lambda_{i,CR} + \lambda_s$), which will have consequences on the predicted CR rates (see below). The $|\Delta G^\circ_{ED}|$ values of the polymer–SMA systems are smaller than those of the polymer–polymer system **BDT-TzBI–NDI2OD-T2**, but because their $\lambda_{i,ED}$ values are also smaller and the electronic couplings larger (for the most stable configurations) their ED rates are relatively similar with the polymer–polymer **BDT-TzBI–NDI2OD-T2** system (see above). The larger $|\Delta G^\circ_{CR}|$ of the polymer–SMA systems, in turn, will lead to the slower CR rates with respect to **BDT-TzBI–NDI2OD-T2** (see below).

After examining the individual CT parameters, the rates for the ED and CR processes of the studied NF PSC systems are presented as a function of λ_s (0.10–0.75 eV) in Fig. 11 and S8.† For all the systems, the ED rates are larger than the CR rates (10^{12} to 10^{14} s^{-1} and below 10^{12} s^{-1}, respectively). Even though no irrevocable conclusions regarding the relative efficiencies of the studied NF PSC systems can be drawn based on their ED rates, which depend highly on the relative orientations of the eD and eA compounds (see below), we can conclude the following. The CR rates of the polymer–SMA systems are predicted to be slower compared to those of the polymer–polymer system, which could be one factor defining the higher efficiencies of the polymer–SMA systems **PDTB-EF-T–ITIC-4F** and **PBDB-T-2F–ITIC-2Cl** compared to those of the polymer–polymer system **PBDT-TzBI–P(NDI2OD-T2)**. The calculated ED rates are consistent with those ($\sim 10^8$ to 10^{12} s^{-1}) predicted for the systems consisting of **BDB-T-2F** and different derivatives of **ITIC** by using the Marcus theory.[47–49] Similarly, the CR rates calculated here are mostly in line with those (10^2–10^{10} s^{-1}) predicted for the complexes of **BDB-T-2F** and **ITIC** derivatives.[47–49] However, vanishingly small CR rates are observed here with the smaller values of λ_s, which could be due to that the CR processes of all the systems occur deep into the Marcus inverted region ($|\Delta G^\circ_{CR}| \gg \lambda_{CR}$).[130] As the Marcus theory may predict underestimated rates in such a case,[49,131] another, *e.g.* the Marcus–Levich–Jortner rate model[132] could be more suitable for calculating the CR rates in these PSC systems.

The relative orientations of the eD and eA compounds (see Tables S8–S10† for the optimized configurations) have a significant influence on the calculated rates, and the different configurations of the same system can have completely different rates. As an example, the DA configuration of the copolymer–SMA system **DTB-EF-T–ITIC-4F**, where the electron-withdrawing end-group of **ITIC-4F** is on the top of the BDT donor unit of **DTB-EF-T**, is predicted to have the fastest ED rate among the studied PSC systems. However, **DTB-EF-T–ITIC-4F** has the slowest ED rate among the studied systems, when the end-group of **ITIC-4F** is on the top of the acceptor unit of **DTB-EF-T** (*i.e.* ester-substituted thiophene; the AA configuration). As other CT parameters of these two configurations are relatively similar (Table 3), the smaller ED rates of the AA configuration can be attributed to its significantly smaller electronic couplings compared to those of the DA configuration.

For the polymer–SMA systems, the energetically more stable configurations have faster ED and CR rates following the same trends as their electronic couplings. However, for the polymer–

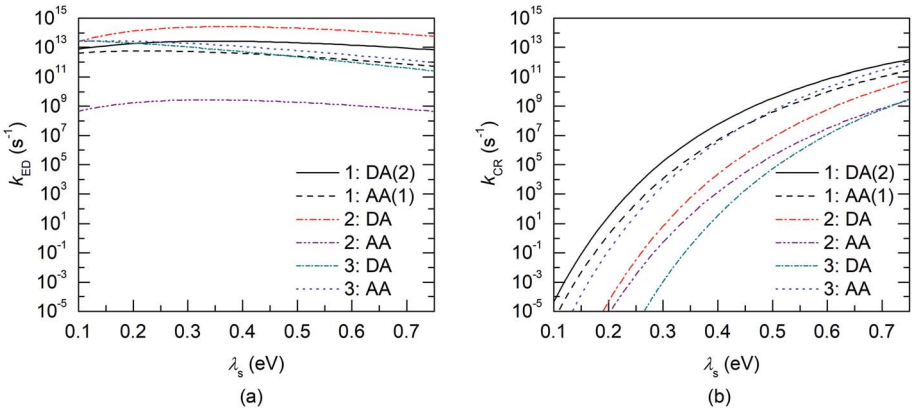

Fig. 11 Evolutions of the charge transfer rates (k_{ED} and k_{CR}) as functions of λ_s (0.1–0.75 eV) for the (a) ED and (b) CR processes of the **BDT-TzBI**–**NDI2OD-T2** (1), **DTB-EF-T**–**ITIC-4F** (2), and **BDB-T-2F**–**ITIC-2Cl** (3) complexes calculated at the OT-ωB97X-D/6-31G** level of theory in blend.

polymer **BDT-TzBI**–**NDI2OD-T2** system, the most stable configuration, *i.e.* the AA(1) configuration, has generally the slowest ED and CR rates among the studied complex configurations of **BDT-TzBI**–**NDI2OD-T2** (Fig. S8†) due to its smaller $|\Delta G^{\circ}_{ED}|$ value and moderate ED electronic couplings. Moreover, based on the larger $|\Delta G^{\circ}_{CR}|$ value of the AA(1) configuration with respect to the other configurations of **BDT-TzBI**–**NDI2OD-T2**, the CR process of AA(1) takes place deeper in the Marcus inverted region leading to the slower CR rates. While we have not included the full-length side groups, which also impact the interfacial orientations and stacking distances of the compounds, our findings complement the experimental findings for the importance of the optimal molecular orientation at the eD–eA interfaces.[37]

Conclusions

In this work, the structural, optoelectronic, and CT characteristics of several eD and eA compounds and their local interfacial eD–eA complexes have been examined with the DFT and TDDFT methods. The chosen compounds are based on some of the most efficient NF PSC systems to date, including both the APSC system and those containing eD copolymers and NF SMAs. We have extended our previous study of multi-state electronic couplings by comparing the two- and multi-state couplings for the ED and CR processes of these systems and exploring the effects of both the tuning of a LRC functional and the inclusion of the dispersion corrections on the electronic coupling values. Finally, the CT rates for the ED and CR processes in the studied NF PSC systems have been calculated using the semi-classical Marcus theory.

The results indicate that the studied eD copolymers **PBDT-TzBI**, **PDTB-EF-T**, and **PBDB-T-2F** have some similar features, such as similar torsions in their backbones and UV-vis absorption profiles. However, the conformational preferences and varying backbone curvatures of these eD copolymers may lead to significant differences in their packing behavior in the blend environment. Moreover, a closer look at the structural deformations caused by ionization and excitation reveal subtle differences in the regions of their backbones, which are affected most by these processes. While all the studied eD copolymer models show a partial intramolecular CT character, the amount of transferred charge density is smaller in **DTB-EF-T** than in **BDT-TzBI** and **BDB-T-2F**. In general, both the twisted backbone structures, which originate from the additional degrees of freedom caused by the thiophene spacers between the donor and acceptor units of the modelled eD copolymers, and the predicted intramolecular CT characteristics are concluded to be beneficial for the performance of the PSCs.

Based on our computational studies of the CT characteristics in various possible face-to-face orientations between the eD and eA compounds in the eD–eA complexes of the NF PSC systems, the following conclusions were reached. In addition to the conventional CT from the eD compound to the eA compound, which is prominent in all NF PSC systems, the CT process is also observed from the eA compound **NDI2OD-T2** to the eD compound, which indicates that **NDI2OD-T2** could contribute to the charge generation in the studied polymer–polymer system. In the polymer–SMA systems, the energetically most favorable configurations have the strongest electronic couplings and the fastest CT rates. However, the positioning of the eA with respect to the eD is predicted to be different in **DTB-EF-T**–**ITIC-4F** and **BDB-T-2F**–**ITIC-2Cl**. In the case of the polymer–polymer system, the most stable configuration leads to smaller electronic couplings and slower CT rates compared to the second most stable configuration. Our results agree with the reports in the literature that the electronic couplings are highly dependent on the relative positioning of the eD and eA compounds which should be carefully controlled to ensure the fast ED rates, but slow CR rates.

The present FCD electronic coupling calculations complement our previous results on the effects of the two- *versus* multi-state treatment on the PSC systems. In this work we observed, that the multi-state FCD electronic couplings seem to be stabilized by including the dispersion corrections in the OT-LRC functional, *i.e.* relatively constant ED and CR couplings are predicted with both the two- and multi-state treatments. While more work would be required to confirm the effect of dispersion corrections on the electronic couplings in other NF

PSC systems, these findings complement our and other's previous statements for the importance of the combined effect of the dispersion corrections and tuned LRC functional when describing the local interfacial characteristics of PSC systems.

The polymer–SMA systems are predicted to have smaller inner reorganization energies for the ED process, which could be one factor explaining their higher efficiencies with respect to the polymer–polymer system. However, the Gibbs free energies for ED are smaller for the polymer–SMA systems than for the polymer–polymer system, which could explain, why no clear trends in ED rates are observed between the studied NF PSC systems. Nevertheless, the calculated ED rates are faster than the CR rates in all systems, which is desirable for working devices. In addition, the CR rates in the polymer–SMA systems are generally slower than in the polymer–polymer system, which could contribute to the higher power conversion efficiencies in the SMA containing systems. The magnitudes of the ED rates are rather constant regardless of the external reorganization energy, which affects the CR rates more pronouncedly. The vanishingly small CR rates associated with the smaller external reorganization energies indicate that comparing the applicability of an alternative CT rate model, *e.g.* the Marcus–Levich–Jortner, could be beneficial, when calculating the CR rates for these types of NF PSC systems.

This work provides more insight into the interplay between the structural, optoelectronic, and CT characteristics of the NF PSC compounds with high PCEs demonstrated in devices. Furthermore, important information about the structural and CT characteristics in both the APC and polymer-SMA type NF PSC systems has been revealed. Overall, the dispersion corrected OT-LRC functional is concluded to be a suitable choice for modeling of the NF PSC systems, especially for calculating the FCD electronic couplings. The findings of this work are beneficial for understanding the working principles of the studied systems and can help in designing and developing more efficient NF PSCs.

Conflicts of interest

The authors declare no competing financial interest.

Acknowledgements

Computing resources provided by the CSC – IT Center for Science Ltd, administrated by the Finnish Ministry of Education, are acknowledged. Financing of this research by the Graduate School of Tampere University of Technology (TUT), the Finnish Cultural Foundation, and the Faculty of Engineering and Natural Sciences of Tampere University is greatly appreciated. Professor Demetrio da Silva Filho and Assistant Professor Lassi Paunonen are acknowledged for allowing a continued use of the codes for analyzing the NTO contributions of the complexes and calculating the multi-state electronic couplings, respectively. We also thank M.Sc. Tech. Maria Pullinen for the information from her calculations of **DTB-EF-T** in her Master's thesis.

References

1 Z. He, C. Zhong, S. Su, M. Xu, H. Wu and Y. Cao, *Nat. Photonics*, 2012, **6**, 591–595.
2 G. Li, R. Zhu and Y. Yang, *Nat. Photonics*, 2012, **6**, 153–161.
3 J. Zhao, Y. Li, G. Yang, K. Jiang, H. Lin, H. Ade, W. Ma and H. Yan, *Nat. Energy*, 2016, **1**, 15027.
4 Y. Jin, Z. Chen, M. Xiao, J. Peng, B. Fan, L. Ying, G. Zhang, X.-F. Jiang, Q. Yin, Z. Liang, F. Huang and Y. Cao, *Adv. Energy Mater.*, 2017, **7**, 1700944.
5 H. Kang, W. Lee, J. Oh, T. Kim, C. Lee and B. J. Kim, *Acc. Chem. Res.*, 2016, **49**, 2424–2434.
6 S. Chen, Y. An, G. K. Dutta, Y. Kim, Z.-G. Zhang, Y. Li and C. Yang, *Adv. Funct. Mater.*, 2017, **27**, 1603564.
7 F. Shen, J. Xu, X. Li and C. Zhan, *J. Mater. Chem. A*, 2018, **6**, 15433–15455.
8 Z.-H. Zhou, T. Maruyama, T. Kanbara, T. Ikeda, K. Ichimura, T. Yamamoto and K. Tokuda, *J. Chem. Soc., Chem. Commun.*, 1991, 1210–1212.
9 E. E. Havinga, W. ten Hoeve and H. Wynberg, *Polym. Bull.*, 1992, **29**, 119–126.
10 H. Zhou, L. Yang and W. You, *Macromolecules*, 2012, **45**, 607–632.
11 F. Würthner and M. Stolte, *Chem. Commun.*, 2011, **47**, 5109–5115.
12 G. Wang, F. S. Melkonyan, A. Facchetti and T. J. Marks, *Angew. Chem., Int. Ed.*, 2019, **58**, 4129–4142.
13 Z. Li, L. Ying, P. Zhu, W. Zhong, N. Li, F. Liu, F. Huang and Y. Cao, *Energy Environ. Sci.*, 2019, **12**, 157–163.
14 L. Zhu, W. Zhong, C. Qiu, B. Lyu, Z. Zhou, M. Zhang, J. Song, J. Xu, J. Wang, J. Ali, W. Feng, Z. Shi, X. Gu, L. Ying, Y. Zhang and F. Liu, *Adv. Mater.*, 2019, **31**, 1902899.
15 X. Guo and M. D. Watson, *Org. Lett.*, 2008, **10**, 5333–5336.
16 T. Jia, J. Zhang, W. Zhong, Y. Liang, K. Zhang, S. Dong, L. Ying, F. Liu, X. Wang, F. Huang and Y. Cao, *Nano Energy*, 2020, **72**, 104718.
17 Y. Lin, J. Wang, Z.-G. Zhang, H. Bai, Y. Li, D. Zhu and X. Zhan, *Adv. Mater.*, 2015, **27**, 1170–1174.
18 G. Zhang, J. Zhao, P. C. Y. Chow, K. Jiang, J. Zhang, Z. Zhu, J. Zhang, F. Huang and H. Yan, *Chem. Rev.*, 2018, **118**, 3447–3507.
19 J. Hou, O. Inganäs, R. H. Friend and F. Gao, *Nat. Mater.*, 2018, **17**, 119–128.
20 H. Sun, F. Chen and Z. K. Chen, *Mater. Today*, 2019, **24**, 94–118.
21 Z. Zheng, Q. Hu, S. Zhang, D. Zhang, J. Wang, S. Xie, R. Wang, Y. Qin, W. Li, L. Hong, N. Liang, F. Liu, Y. Zhang, Z. Wei, Z. Tang, T. P. Russell, J. Hou and H. Zhou, *Adv. Mater.*, 2018, **30**, 1801801.
22 Y. Cui, H. Yao, L. Hong, T. Zhang, Y. Xu, K. Xian, B. Gao, J. Qin, J. Zhang, Z. Wei and J. Hou, *Adv. Mater.*, 2019, **31**, 1808356.
23 H. Yao, Y. Cui, D. Qian, C. S. Ponseca, A. Honarfar, Y. Xu, J. Xin, Z. Chen, L. Hong, B. Gao, R. Yu, Y. Zu, W. Ma, P. Chabera, T. Pullerits, A. Yartsev, F. Gao and J. Hou, *J. Am. Chem. Soc.*, 2019, **141**, 7743–7750.

24 Q. Liu, Y. Jiang, K. Jin, J. Qin, J. Xu, W. Li, J. Xiong, J. Liu, Z. Xiao, K. Sun, S. Yang, X. Zhang and L. Ding, *Sci. Bull.*, 2020, **65**, 272–275.
25 J. Yuan, Y. Zhang, L. Zhou, G. Zhang, H. L. Yip, T. K. Lau, X. Lu, C. Zhu, H. Peng, P. A. Johnson, M. Leclerc, Y. Cao, J. Ulanski, Y. Li and Y. Zou, *Joule*, 2019, **3**, 1140–1151.
26 P. Cheng, G. Li, X. Zhan and Y. Yang, *Nat. Photonics*, 2018, **12**, 131–142.
27 B. Fan, L. Ying, Z. Wang, B. He, X. F. Jiang, F. Huang and Y. Cao, *Energy Environ. Sci.*, 2017, **10**, 1243–1251.
28 L. Lan, Z. Chen, Q. Hu, L. Ying, R. Zhu, F. Liu, T. P. Russell, F. Huang and Y. Cao, *Adv. Sci.*, 2016, **3**, 1600032.
29 S. Li, L. Ye, W. Zhao, H. Yan, B. Yang, D. Liu, W. Li, H. Ade and J. Hou, *J. Am. Chem. Soc.*, 2018, **140**, 7159–7167.
30 L. Zhan, S. Li, S. Zhang, X. Chen, T. K. Lau, X. Lu, M. Shi, C. Z. Li and H. Chen, *ACS Appl. Mater. Interfaces*, 2018, **10**, 42444–42452.
31 M. Zhang, X. Guo, W. Ma, H. Ade and J. Hou, *Adv. Mater.*, 2015, **27**, 4655–4660.
32 Poly[(4,8-bis[5-(2-ethylhexyl)-4-fluoro-2-thienyl)benzo[1,2-*b*:4,5-*b*′]dithiophene-2,6-diyl]-2,5-thiophenediyl(5,7-bis(2-ethylhexyl)-4,8-dioxo-4*H*,8*H*-benzo[1,2-*c*:4,5-*c*′]dithiophene-1,3-diyl)-2,5-thiophenediyl], **PBDB-T-2F** at Sigma-Aldrich, available at: https://www.sigmaaldrich.com/catalog/product/aldrich/906336?lang=fi&region=FI, accessed 20/05/2020.
33 H. Zhang, H. Yao, J. Hou, J. Zhu, J. Zhang, W. Li, R. Yu, B. Gao, S. Zhang and J. Hou, *Adv. Mater.*, 2018, **30**, 1800613.
34 Y. Ie, J. Huang, Y. Uetani, M. Karakawa and Y. Aso, *Macromolecules*, 2012, **45**, 4564–4571.
35 D. Qian, L. Ye, M. Zhang, Y. Liang, L. Li, Y. Huang, X. Guo, S. Zhang, Z. Tan and J. Hou, *Macromolecules*, 2012, **45**, 9611–9617.
36 D. Gedefaw, M. Tessarolo, W. Zhuang, R. Kroon, E. Wang, M. Bolognesi, M. Seri, M. Muccini and M. R. Andersson, *Polym. Chem.*, 2014, **5**, 2083–2093.
37 C. Lee, S. Lee, G.-U. Kim, W. Lee and B. J. Kim, *Chem. Rev.*, 2019, **119**, 8028–8086.
38 Q. Zhang, M. A. Kelly, N. Bauer and W. You, *Acc. Chem. Res.*, 2017, **50**, 2401–2409.
39 L. Benatto and M. Koehler, *J. Phys. Chem. C*, 2019, **123**, 6395–6406.
40 L. Benatto, C. F. N. Marchiori, C. Moyses Araujo and M. Koehler, *J. Mater. Chem. C*, 2019, **7**, 12180–12193.
41 Q. Wang, Y. Li, P. Song, R. Su, F. Ma, Y. Yang, Q. Wang, Y. Li, P. Song, R. Su, F. Ma and Y. Yang, *Polymers*, 2017, **9**, 692.
42 Y. Cui, H. Yao, J. Zhang, T. Zhang, Y. Wang, L. Hong, K. Xian, B. Xu, S. Zhang, J. Peng, Z. Wei, F. Gao and J. Hou, *Nat. Commun.*, 2019, **10**, 1–8.
43 L. Benatto and M. Koehler, *J. Phys. Chem. C*, 2019, **123**, 6395–6406.
44 G. Han, Y. Guo, X. Ma and Y. Yi, *Sol. RRL*, 2018, **2**, 1800190.
45 G. Han and Y. Yi, *Adv. Theory Simul.*, 2018, **1**, 1800091.
46 J. Lee, E. M. Go, S. Dharmapurikar, J. Xu, S. M. Lee, M. Jeong, K. C. Lee, J. Oh, Y. Cho, C. Zhang, M. Xiao, S. K. Kwak and C. Yang, *J. Mater. Chem. A*, 2019, **7**, 18468–18479.
47 Q.-Q. Pan, S.-B. Li, Y.-C. Duan, Y. Wu, J. Zhang, Y. Geng, L. Zhao and Z.-M. Su, *Phys. Chem. Chem. Phys.*, 2017, **19**, 31227–31235.
48 Q.-Q. Pan, S.-B. Li, Y. Wu, Y. Geng, M. Zhang and Z.-M. Su, *Org. Electron.*, 2018, **53**, 308–314.
49 T. Wang and J.-L. Brédas, *Matter*, 2020, **2**, 119–135.
50 G. Han, Y. Guo, X. Song, Y. Wang and Y. Yi, *J. Mater. Chem. C*, 2017, **5**, 4852–4857.
51 J.-L. Brédas, V. Coropceanu, C. Doiron, Y. T. Fu, T. Körzdörfer, L. Pandey, C. Risko, J. Sears, B. Yang, Y. Yi and C. Zhang, Modeling the electronic and optical processes in organic solar cells: density functional theory and beyond, in *Organic Solar Cells: Fundamentals, Devices, and Upscaling*, ed. B. P. Rand and H. Richter, CRC Press, Taylor & Francis Group, LLC, Boca Raton, 2014, pp. 537–588.
52 V. Coropceanu, J. Cornil, D. A. da Silva Filho, Y. Olivier, R. Silbey and J.-L. Brédas, *Chem. Rev.*, 2007, **107**, 926–952.
53 C.-P. Hsu, *Acc. Chem. Res.*, 2009, **42**, 509–518.
54 H. Oberhofer, K. Reuter and J. Blumberger, *Chem. Rev.*, 2017, **117**, 10319–10357.
55 P. Song, Y. Li, F. Ma, T. Pullerits and M. Sun, *Chem. Rec.*, 2016, **16**, 734–753.
56 A. A. Voityuk and N. Rösch, *J. Chem. Phys.*, 2002, **117**, 5607–5616.
57 R. J. Cave and M. D. Newton, *Chem. Phys. Lett.*, 1996, **249**, 15–19.
58 R. J. Cave and M. D. Newton, *J. Chem. Phys.*, 1997, **106**, 9213–9226.
59 Y. Li, T. Pullerits, M. Zhao and M. Sun, *J. Phys. Chem. C*, 2011, **115**, 21865–21873.
60 Y. Li, Y. Feng and M. Sun, *Sci. Rep.*, 2015, **5**, 13970.
61 D. Qian, Z. Zheng, H. Yao, W. Tress, T. R. Hopper, S. Chen, S. Li, J. Liu, S. Chen, J. Zhang, X.-K. Liu, B. Gao, L. Ouyang, Y. Jin, G. Pozina, I. A. Buyanova, W. M. Chen, O. Inganäs, V. Coropceanu, J.-L. Brédas, H. Yan, J. Hou, F. Zhang, A. A. Bakulin and F. Gao, *Nat. Mater.*, 2018, **17**, 703–709.
62 T. Wang, X.-K. Chen, A. Ashokan, Z. Zheng, M. K. Ravva and J.-L. Brédas, *Adv. Funct. Mater.*, 2018, **28**, 1705868.
63 M. Rust, J. Lappe and R. J. Cave, *J. Phys. Chem. A*, 2002, **106**, 3930–3940.
64 C.-H. Yang and C.-P. Hsu, *J. Chem. Phys.*, 2013, **139**, 154104.
65 T. Kastinen, M. Niskanen, C. Risko, O. Cramariuc and T. I. Hukka, *Phys. Chem. Chem. Phys.*, 2016, **18**, 27654–27670.
66 T. Kastinen, D. A. Da Silva Filho, L. Paunonen, M. Linares, L. A. Ribeiro Junior, O. Cramariuc and T. I. Hukka, *Phys. Chem. Chem. Phys.*, 2019, **21**, 25606–25625.
67 T. Kim, J. H. Kim, T. E. Kang, C. Lee, H. Kang, M. Shin, C. Wang, B. Ma, U. Jeong, T. S. Kim and B. J. Kim, *Nat. Commun.*, 2015, **6**, 8547.
68 K. Do, M. K. Ravva, T. Wang and J.-L. Brédas, *Chem. Mater.*, 2017, **29**, 346–354.
69 C.-R. Zhang, J. S. Sears, B. Yang, S. G. Aziz, V. Coropceanu and J.-L. Brédas, *J. Chem. Theory Comput.*, 2014, **10**, 2379–2388.

70 L. Pandey, C. Doiron, J. S. Sears and J.-L. Brédas, *Phys. Chem. Chem. Phys.*, 2012, **14**, 14243–14248.
71 M. Niskanen and T. I. Hukka, *Phys. Chem. Chem. Phys.*, 2014, **16**, 13294–13305.
72 J.-D. Chai and M. Head-Gordon, *Phys. Chem. Chem. Phys.*, 2008, **10**, 6615–6620.
73 J. P. Perdew, K. Burke and M. Ernzerhof, *Phys. Rev. Lett.*, 1996, **77**, 3865–3868.
74 C. Adamo and V. Barone, *J. Chem. Phys.*, 1999, **110**, 6158–6170.
75 J. P. Perdew, K. Burke and M. Ernzerhof, *Phys. Rev. Lett.*, 1997, **78**, 1396.
76 D. Niedzialek, I. Duchemin, T. B. De Queiroz, S. Osella, A. Rao, R. Friend, X. Blase, S. Kümmel and D. Beljonne, *Adv. Funct. Mater.*, 2015, **25**, 1972–1984.
77 M. J. Frisch, G. W. Trucks, H. B. Schlegel, G. E. Scuseria, M. A. Robb, J. R. Cheeseman, G. Scalmani, V. Barone, G. A. Petersson, H. Nakatsuji, X. Li, M. Caricato, A. V. Marenich, J. Bloino, B. G. Janesko, R. Gomperts, B. Mennucci, H. P. Hratchian, J. V. Ortiz, A. F. Izmaylov, J. L. Sonnenberg, D. Williams-Young, F. Ding, F. Lipparini, F. Egidi, J. Goings, B. Peng, A. Petrone, T. Henderson, D. Ranasinghe, V. G. Zakrzewski, J. Gao, N. Rega, G. Zheng, W. Liang, M. Hada, M. Ehara, K. Toyota, R. Fukuda, J. Hasegawa, M. Ishida, T. Nakajima, Y. Honda, O. Kitao, H. Nakai, T. Vreven, K. Throssell, J. A. Montgomery Jr, J. E. Peralta, F. Ogliaro, M. J. Bearpark, J. J. Heyd, E. N. Brothers, K. N. Kudin, V. N. Staroverov, T. A. Keith, R. Kobayashi, J. Normand, K. Raghavachari, A. P. Rendell, J. C. Burant, S. S. Iyengar, J. Tomasi, M. Cossi, J. M. Millam, M. Klene, C. Adamo, R. Cammi, J. W. Ochterski, R. L. Martin, K. Morokuma, O. Farkas, J. B. Foresman and D. J. Fox, *Gaussian 16, Revision B.01*, Gaussian, Inc., Wallingford CT, 2016.
78 Y. Shao, Z. Gan, E. Epifanovsky, A. T. B. Gilbert, M. Wormit, J. Kussmann, A. W. Lange, A. Behn, J. Deng, X. Feng, D. Ghosh, M. Goldey, P. R. Horn, L. D. Jacobson, I. Kaliman, R. Z. Khaliullin, T. Kuś, A. Landau, J. Liu, E. I. Proynov, Y. M. Rhee, R. M. Richard, M. A. Rohrdanz, R. P. Steele, E. J. Sundstrom, H. L. Woodcock III, P. M. Zimmerman, D. Zuev, B. Albrecht, E. Alguire, B. Austin, G. J. O. Beran, Y. A. Bernard, E. Berquist, K. Brandhorst, K. B. Bravaya, S. T. Brown, D. Casanova, C.-M. Chang, Y. Chen, S. H. Chien, K. D. Closser, D. L. Crittenden, M. Diedenhofen, R. A. DiStasio, H. Do, A. D. Dutoi, R. G. Edgar, S. Fatehi, L. Fusti-Molnar, A. Ghysels, A. Golubeva-Zadorozhnaya, J. Gomes, M. W. D. Hanson-Heine, P. H. P. Harbach, A. W. Hauser, E. G. Hohenstein, Z. C. Holden, T.-C. Jagau, H. Ji, B. Kaduk, K. Khistyaev, J. Kim, J. Kim, R. A. King, P. Klunzinger, D. Kosenkov, T. Kowalczyk, C. M. Krauter, K. U. Lao, A. D. Laurent, K. V. Lawler, S. V. Levchenko, C. Y. Lin, F. Liu, E. Livshits, R. C. Lochan, A. Luenser, P. Manohar, S. F. Manzer, S.-P. Mao, N. Mardirossian, A. V. Marenich, S. A. Maurer, N. J. Mayhall, E. Neuscamman, C. M. Oana, R. Olivares-Amaya, D. P. O'Neill, J. A. Parkhill, T. M. Perrine, R. Peverati, A. Prociuk, D. R. Rehn, E. Rosta, N. J. Russ, S. M. Sharada, S. Sharma, D. W. Small, A. Sodt, T. Stein, D. Stück, Y.-C. Su, A. J. W. Thom, T. Tsuchimochi, V. Vanovschi, L. Vogt, O. Vydrov, T. Wang, M. A. Watson, J. Wenzel, A. White, C. F. Williams, J. Yang, S. Yeganeh, S. R. Yost, Z.-Q. You, I. Y. Zhang, X. Zhang, Y. Zhao, B. R. Brooks, G. K. L. Chan, D. M. Chipman, C. J. Cramer, W. A. Goddard III, M. S. Gordon, W. J. Hehre, A. Klamt, H. F. Schaefer III, M. W. Schmidt, C. D. Sherrill, D. G. Truhlar, A. Warshel, X. Xu, A. Aspuru-Guzik, R. Baer, A. T. Bell, N. A. Besley, J.-D. Chai, A. Dreuw, B. D. Dunietz, T. R. Furlani, S. R. Gwaltney, C.-P. Hsu, Y. Jung, J. Kong, D. S. Lambrecht, W. Liang, C. Ochsenfeld, V. A. Rassolov, L. V. Slipchenko, J. E. Subotnik, T. Van Voorhis, J. M. Herbert, A. I. Krylov, P. M. W. Gill and M. Head-Gordon, *Mol. Phys.*, 2015, **113**, 184–215.
79 L. Kronik, T. Stein, S. Refaely-Abramson and R. Baer, *J. Chem. Theory Comput.*, 2012, **8**, 1515–1531.
80 T. Stein, L. Kronik and R. Baer, *J. Am. Chem. Soc.*, 2009, **131**, 2818–2820.
81 B. Yang, Y. Yi, C.-R. Zhang, S. G. Aziz, V. Coropceanu and J.-L. Brédas, *J. Phys. Chem. C*, 2014, **118**, 27648–27656.
82 V. Barone and M. Cossi, *J. Phys. Chem. A*, 1998, **102**, 1995–2001.
83 M. Cossi, N. Rega, G. Scalmani and V. Barone, *J. Comput. Chem.*, 2003, **24**, 669–681.
84 X.-K. Chen, M. K. Ravva, H. Li, S. M. Ryno and J.-L. Brédas, *Adv. Energy Mater.*, 2016, **6**, 1601325.
85 G. Han and Y. Yi, *J. Phys. Chem. Lett.*, 2019, **10**, 2911–2918.
86 R. L. Martin, *J. Chem. Phys.*, 2003, **118**, 4775–4777.
87 A. Dreuw and M. Head-Gordon, *Chem. Rev.*, 2005, **105**, 4009–4037.
88 P. Ros and G. C. A. Schuit, *Theor. Chim. Acta*, 1966, **4**, 1–12.
89 Multiwfn 3.6, available at: http://sobereva.com/multiwfn/, accessed 05/01/2020.
90 T. Lu and F. Chen, *J. Comput. Chem.*, 2012, **33**, 580–592.
91 T. Lu and F. Chen, *Acta Chim. Sin.*, 2011, **69**, 2393–2406.
92 G. A. Zhurko, Chemcraft - graphical program for visualization of quantum chemistry computations, Ivanovo, Russia, 2005, available at: http://www.chemcraftprog.com, accessed 24/05/2020.
93 R. A. Marcus, *J. Chem. Phys.*, 1956, **24**, 966–978.
94 R. A. Marcus and N. Sutin, *Biochim. Biophys. Acta, Rev. Bioenerg.*, 1985, **811**, 265–322.
95 R. A. Marcus, *Rev. Mod. Phys.*, 1993, **65**, 599–610.
96 M. D. Newton, *Chem. Rev.*, 1991, **91**, 767–792.
97 C. F. Huang, S. L. Wu, Y. F. Huang, Y. C. Chen, S. T. Chang, T. Y. Wu, K. Y. Wu, W. T. Chuang and C. L. Wang, *Chem. Mater.*, 2016, **28**, 5175–5190.
98 A. Wadsworth, M. Moser, A. Marks, M. S. Little, N. Gasparini, C. J. Brabec, D. Baran and I. McCulloch, *Chem. Soc. Rev.*, 2019, **48**, 1596–1625.
99 N. E. Jackson, B. M. Savoie, K. L. Kohlstedt, M. Olvera de la Cruz, G. C. Schatz, L. X. Chen and M. A. Ratner, *J. Am. Chem. Soc.*, 2013, **135**, 10475–10483.

100 T. Kastinen, M. Niskanen, C. Risko, O. Cramariuc and T. I. Hukka, *J. Phys. Chem. A*, 2016, **120**, 1051–1064.
101 I. Osaka, T. Abe, S. Shinamura and K. Takimiya, *J. Am. Chem. Soc.*, 2011, **133**, 6852–6860.
102 E. Giussani, D. Fazzi, L. Brambilla, M. Caironi and C. Castiglioni, *Macromolecules*, 2013, **46**, 2658–2670.
103 D. Fazzi, M. Caironi and C. Castiglioni, *J. Am. Chem. Soc.*, 2011, **133**, 19056–19059.
104 T. Schuettfort, S. Huettner, S. Lilliu, J. E. MacDonald, L. Thomsen and C. R. McNeill, *Macromolecules*, 2011, **44**, 1530–1539.
105 V. Lemaur, L. Muccioli, C. Zannoni, D. Beljonne, R. Lazzaroni, J. Cornil and Y. Olivier, *Macromolecules*, 2013, **46**, 8171–8178.
106 T. J. Aldrich, M. Matta, W. Zhu, S. M. Swick, C. L. Stern, G. C. Schatz, A. Facchetti, F. S. Melkonyan and T. J. Marks, *J. Am. Chem. Soc.*, 2019, **141**, 3274–3287.
107 Z. Zhang, J. Yu, X. Yin, Z. Hu, Y. Jiang, J. Sun, J. Zhou, F. Zhang, T. P. Russell, F. Liu and W. Tang, *Adv. Funct. Mater.*, 2018, **28**, 1705095.
108 C. Van Dyck, T. J. Marks and M. A. Ratner, *ACS Nano*, 2017, **11**, 5970–5981.
109 J. Casado, *Top. Curr. Chem.*, 2017, **375**, 1–40.
110 S. Suramitr, W. Meeto, P. Wolschann and S. Hannongbua, *Theor. Chem. Acc.*, 2010, **125**, 35–44.
111 T. Körzdörfer, R. M. Parrish, J. S. Sears, C. D. Sherrill and J.-L. Brédas, *J. Chem. Phys.*, 2012, **137**, 124305.
112 W. Porzio, G. Scavia, L. Barba, G. Arrighetti and C. R. McNeill, *Eur. Polym. J.*, 2014, **61**, 172–185.
113 Y. Olivier, D. Niedzialek, V. Lemaur, W. Pisula, K. Müllen, U. Koldemir, J. R. Reynolds, R. Lazzaroni, J. Cornil and D. Beljonne, *Adv. Mater.*, 2014, **26**, 2119–2136.
114 N. E. Jackson, K. L. Kohlstedt, B. M. Savoie, M. Olvera de la Cruz, G. C. Schatz, L. X. Chen and M. A. Ratner, *J. Am. Chem. Soc.*, 2015, **137**, 6254–6262.
115 W. Zhao, S. Li, H. Yao, S. Zhang, Y. Zhang, B. Yang and J. Hou, *J. Am. Chem. Soc.*, 2017, **139**, 7148–7151.
116 M. Caironi, M. Bird, D. Fazzi, Z. Chen, R. Di Pietro, C. Newman, A. Facchetti and H. Sirringhaus, *Adv. Funct. Mater.*, 2011, **21**, 3371–3381.
117 E. F. Oliveira and F. C. Lavarda, *Polymer*, 2016, **99**, 105–111.
118 C. Risko, M. D. McGehee and J.-L. Brédas, *Chem. Sci.*, 2011, **2**, 1200–1218.
119 B. Fan, L. Ying, P. Zhu, F. Pan, F. Liu, J. Chen, F. Huang and Y. Cao, *Adv. Mater.*, 2017, **29**, 1703906.
120 A. Yin, D. Zhang, S. H. Cheung, S. K. So, Z. Fu, L. Ying, F. Huang, H. Zhou and Y. Zhang, *J. Mater. Chem. C*, 2018, **6**, 7855–7863.
121 G. Han, Y. Guo, X. Ma and Y. Yi, *Sol. RRL*, 2018, **2**, 1800190.
122 D. M. Stoltzfus, J. E. Donaghey, A. Armin, P. E. Shaw, P. L. Burn and P. Meredith, *Chem. Rev.*, 2016, **116**, 12920–12955.
123 A. A. Bakulin, A. Rao, V. G. Pavelyev, P. H. M. Van Loosdrecht, M. S. Pshenichnikov, D. Niedzialek, J. Cornil, D. Beljonne and R. H. Friend, *Science*, 2012, **335**, 1340–1344.
124 S. Chen, S. M. Lee, J. Xu, J. Lee, K. C. Lee, T. Hou, Y. Yang, M. Jeong, B. Lee, Y. Cho, S. Jung, J. Oh, Z. G. Zhang, C. Zhang, M. Xiao, Y. Li and C. Yang, *Energy Environ. Sci.*, 2018, **11**, 2569–2580.
125 L. Pandey, PhD thesis, Georgia Institute of Technology, 2013.
126 J. L. Brédas, D. Beljonne, V. Coropceanu and J. Cornil, *Chem. Rev.*, 2004, **104**, 4971–5003.
127 X.-K. Chen, M. K. Ravva, H. Li, S. M. Ryno and J.-L. Brédas, *Adv. Energy Mater.*, 2016, **6**, 1601325.
128 Y. Yi, V. Coropceanu and J.-L. Brédas, *J. Mater. Chem.*, 2011, **21**, 1479–1486.
129 W. Li, L. Ye, S. Li, H. Yao, H. Ade and J. Hou, *Adv. Mater.*, 2018, **30**, 1707170.
130 V. Lemaur, M. Steel, D. Beljonne, J.-L. Brédas and J. Cornil, *J. Am. Chem. Soc.*, 2005, **127**, 6077–6086.
131 T. Unger, S. Wedler, F.-J. Kahle, U. Scherf, H. Bässler and A. Köhler, *J. Phys. Chem. C*, 2017, **121**, 22739–22752.
132 J. Jortner, *J. Chem. Phys.*, 1976, **64**, 4860–4867.